ACS OMEGA

Open Access

http://pubs.acs.org/journal/acsodf

Article

In Silico and *In Vitro* Analyses to Repurpose Quercetin as a Human Pancreatic α-Amylase Inhibitor

Bimal K. Raut, Siddha Raj Upadhyaya, Jyoti Bashyal, and Niranjan Parajuli*

Cite This: *ACS Omega* 2023, 8, 43617−43631

Read Online

ACCESS | Metrics & More | Article Recommendations | Supporting Information

ABSTRACT: Human pancreatic α-amylase (HPA), situated at the apex of the starch digestion hierarchy, is an attractive therapeutic approach to precisely regulate blood glucose levels, thereby efficiently managing diabetes. Polyphenols offer a natural and multifaceted approach to moderate postprandial sugar spikes, with their slight modulation in carbohydrate digestion and potential secondary benefits, such as antioxidant and anti-inflammatory effects. Taking into consideration the unfavorable side effects of currently available commercial medications, we aimed to study a library of polyphenols attributed to their remarkable antidiabetic properties and screened the most potent HPA inhibitor *via* a comprehensive *in silico* study encompassing molecular docking, molecular mechanics with generalized Born and surface area solvation (MM/GBSA) calculation, molecular dynamics (MD) simulation, density functional theory (DFT) study, and pharmacokinetic properties followed by an *in vitro* assay. Significant hydrogen bonding with the catalytic triad residues of HPA, prominent MM/GBSA binding energy of −27.03 kcal/mol, and the stable nature of the protein−ligand complex with regard to 100 ns MD simulation screened quercetin as the best HPA inhibitor. Additionally, quercetin showed strong reactivity in the substrate-binding pocket of HPA and exhibited favorable pharmacokinetic properties with a considerable inhibitory concentration (IC_{50}) of 57.37 ± 0.9 μg/mL against α-amylase. This study holds prospects for HPA inhibition and suggests quercetin as an approach to therapy for diabetes; however, it is imperative to conduct further research.

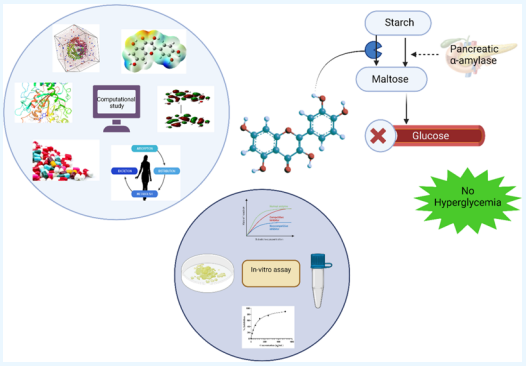

1. INTRODUCTION

α-Amylase (α-1,4-glucan-4-glucanohydrolase) (E.C. 3.2.1.1), belonging to the glycosyl hydrolase family 13, serves a significant role in the catalytic breakdown of α-(1,4)-glycosidic bonds in starch through hydrolysis.[1,2] The mechanism of metabolizing starch in humans commences with the activity of human salivary α-amylase (HSA), an enzyme that hydrolyzes polymeric starch into shorter oligomers. The majority of starch is subjected to digestion by abundant pancreatic amylase, which is secreted into the duodenal portion of the small intestine. The suppression of the HPA enzymatic function presents straightforward avenues to mitigate postprandial hyperglycemia by regulating starch breakdown.

Type 2 diabetes mellitus (T2D), the most commonly encountered form of diabetes, is associated with postprandial hyperglycemia. The global prevalence of diabetes mellitus currently impacts more than 536.6 million individuals, with projections indicating a potential increase to 643 million by 2030 and 783.2 million by 2045.[3] To reduce the prevalence of T2D-related pathophysiologies, nearly 65 medicines have been clinically authorized.[4] Due to the unfortunate reciprocal interplay between gut microbiota and antidiabetic medications, frequent utilization of these medications induces gastrointestinal complications caused by various factors including anaerobic fermentation in the lower gut, ultimately resulting in suboptimal patient adherence.[5−7] The HPA, situated at the apex of the starch digestion hierarchy, has the potential to effectively regulate blood glucose levels quantitatively while minimizing the specificity issues that currently exist with α-glucosidase inhibitors.

HPA catalyzes starch hydrolysis by a double displacement method involving two distinct steps; the initial step, known as the glycosylation step, entails the cleavage of the glycosidic bond, ultimately leading to covalent intermediate formation. The addition of a water molecule within the subsequent stage (deglycosylation) completes the hydrolysis of the carbohydrate by releasing the covalent intermediate between the enzyme and the substrate.[8,9] The conserved catalytic residues ASP197, GLU233, and ASP300 responsible for facilitating carbohydrate hydrolysis are of paramount importance in the process of hydrolyzing glycosidic bonds present in carbohydrates. Numerous studies have elucidated diverse inhibitory mecha-

Received: July 15, 2023
Revised: October 20, 2023
Accepted: October 27, 2023
Published: November 10, 2023

nisms that are responsible for the actions of well-established α-amylase inhibitors. These mechanisms encompass the establishment of hydrogen bonds with the catalytic triad (ASP197, GLU233, and ASP300) and other catalytic residues, interacting at sites distinct from the active site, and the establishment of covalent bonds with enzymes.[10] The regulation of acid−base catalysis is facilitated by the residue GLU233, while coordination concerning the optimal substrate orientation in the binding site is carried out by ASP300. Additionally, ASP197 plays an important role in intervening in the nucleophilic process.[11]

The molecular frameworks of plant-based secondary metabolites have an extensive record of serving as viable medicinal chemistry and drug development bases. Incorporating these chemotypes into chemical collections for screening and attaining selective target activation, inhibition, and modulation has recently seen a resurgence in research.[12] Polyphenols' ability to inhibit α-amylase is greatly influenced by their molecular structure, specifically by the substituent (namely, hydroxyl and methoxy) of the aromatic rings imparting unique molecular characteristics, including but not limited to polarity, stability, and binding. Research findings from both *in vivo* and *in vitro* studies provide substantial evidence supporting the assertion that flavonoids, the most prominent subclasses of polyphenols, have a notable impact on the management of T2D through various mechanisms, improving the glucose metabolism,[13] disrupting the amyloid assembly pathway, and thereby impeding the formation of amylin aggregates,[14] resulting in pancreatic β-cell apoptosis.[15] A longitudinal link between increased flavonoid intake and a lower incidence of diabetes supports the intriguing idea that adding bioactive ingredients with inhibitory activity against digestive enzymes to food products can delay the digestion of carbohydrates.[16]

Computational methodologies can be employed to unveil the mechanism of action of potential pharmaceuticals in the human organism, encompassing predicting outcomes of drug−protein interactions, and scrutiny of biological pathways and functions,[17−19] thereby identifying potent metabolites that could be transformed into promising HPA inhibitors. Herein, to infer the aforementioned potentially novel target sites, we devised a computational framework study that encompasses docking, molecular mechanics with generalized Born and surface area solvation (MM/GBSA), molecular dynamics (MD) simulation, density functional theory (DFT), pharmacokinetic, and toxicity analyses to predict the effective roles of polyphenols in the inhibition of α-amylase. The inhibitors that exhibit efficacious binding and interaction poses with the catalytic triad residue and possess formidable stability with HPA concerning root-mean-square deviation (RMSD), root-mean-square fluctuation (RMSF), radius of gyration (R_g), solvent-accessible surface area (SASA), and hydrogen (H)-bond will proficiently bind with the aimed enzyme with potent reactivity and kinetic stability, thus efficaciously regulating hyperglycemia. To better understand the credibility of the computational analysis outcomes, an analysis was undertaken to explore the inhibitory effect along with the mechanism of action against porcine pancreatic α-amylase (PPA) through an inhibition assay. Employing enhanced comprehension of the inhibitory mechanism, the findings of this investigation will clarify an approach for the strategic suppression of α-amylase inhibition by specific metabolites.

2. RESULTS AND DISCUSSION

2.1. Quality of Protein and Its Validation. The parameter known as the "overall quality factor" for nonbonded atomic interactions, ERRAT, quantifies the level of quality, with higher values denoting better quality. For high-quality models, the acceptable range is > 50; for high-resolution structures, the acceptable range is 95% or higher; and for low-resolution structures, the acceptable range is an average quality factor of around 91%.[20,21] The current HPA was predicted to have an overall quality factor of 97.7178 according to the ERRAT server, demonstrating the protein to be of high quality (Supporting Information, Figure S1).

2.2. Identification of the Binding Site. Utilizing SiteMap, the authenticity of the catalytic site of the receptor protein was verified. It displayed the amino acid residues TRP58, TRP59, TRP62, GLN63, HIS101, TYR151, LEU162, LEU165, ARG195, ASP197, ALA198, LYS200, HIS201, GLU233, VAL234, ILE235, PHE265, ASN298, HIE299, ASP300, HIE305, and ALA307 in the binding site region (Supporting Information, Figure S2 and Table S1), thereby verifying the catalytic sites. Furthermore, these binding sites were found to be in accordance with the literature predicted by the same tool SiteMap with regard to the HPA protein.[22] The SiteScore utilized to assess the ability of a drug to bind to a target site and to identify specific binding sites[23] was found to be 0.992 (∼1). The Dscore value of 1.012, which is >0.7, manifested the binding site to be druggable.[24] Similarly, the catalytic region was assessed in terms of volume, balance, and donor/acceptor value in the catalytic region, which aligns with the established threshold.[25]

2.3. Molecular Docking, MM/GBSA Calculation, and Molecular Dynamics Simulation. Employing molecular docking and MD simulation, a powerful approach in drug discovery, the prediction of enzyme inhibitors gains significant traction as it enables a detailed understanding of their interaction and potential efficacy.[26,27] Polyphenols are structurally varied molecules with the ability to develop a variety of interactions with enzymes and are one of the most extensively researched constituents to moderate carbohydrate digestion, leading to controlled blood sugar levels, making them valuable for diabetes control and general metabolic health. Specifically, the multiple hydroxyl groups attributed to antioxidant properties maintaining insulin sensitivity,[28] inhibition of the enzyme involved in carbohydrate digestion and metabolism,[29] receptor modulation, broad mechanism of action *via* multiple pathways,[30,31] pleiotropic effects,[32] and prebiotic nature[33] make polyphenols a viable metabolite to study comprehensively. Initially, the selected polyphenols were screened based on molecular docking encompassing a binding score with competitive interaction and MD simulation to explore the optimal HPA inhibitor.

With regard to molecular docking, precision and firmness were ensured initially using redocking approaches. The RMSD of less than 2 Å (0.1766 Å) of the cognate ligands verified the protocol.[34] The superimposition of the cognate ligand is displayed in Figure S3 (Supporting Information). Following the successful validation of the docking protocol, the chosen secondary metabolites were subjected to docking within the active site of HPA. Consequently, an assessment of the ligand interactions, docking score, and MM/GBSA value was evaluated, as presented in Table 1. These compounds exhibited docking scores of −0.67 to −7.54 kcal/mol, glide scores from

https://doi.org/10.1021/acsomega.3c05082
ACS Omega 2023, 8, 43617−43631

Table 1. Binding Scores of Selected Metabolites

compounds	docking score (kcal/mol)	glide score (kcal/mol)	MM/GBSA dG bind
apigenin	−5.80	−6.15	−17.15
caffeic acid	−4.30	−4.30	7.91
catechin	−7.43	−7.43	−13.79
chlorogenic acid	−0.67	−0.67	7.42
ellagic acid	−7.54	−7.62	−23.89
epicatechin	−7.16	−7.16	−16.95
isovitexin	−3.86	−3.92	−17.47
kaempferol	−4.69	−6.45	−17.59
protocatechuic acid	−3.59	−3.59	11.70
quercetin	−6.63	−7.00	−27.03
scutellarin	−4.09	−4.09	−8.89
vitexin	−7.05	−7.13	−21.99
acarbose	−7.84	−8.17	−26.69

−0.67 up to −7.62 kcal/mol, and MM/GBSA binding energies in the range of 7.42 to −27.03 as compared to −7.84 kcal/mol docking score, −8.17 glide score kcal/mol, and −26.69 kcal/mol MM/GBSA binding energy of the standard compound acarbose.

Based on the binding score, compounds like caffeic acid, chlorogenic acid, and protocatechuic acid showed poor results, signifying a weak interaction between the protein and the ligand, while compounds such as apigenin, catechin, epicatechin, isovitexin, kaempferol, and scutellarin exhibited moderate binding scores. Meanwhile, with a promising docking score, glide score, and MM/GBSA, the three metabolites—ellagic acid, quercetin, and vitexin—showed the highest score, thereby indicating a strong interaction between HPA and these aforementioned metabolites. The result was correlated with the findings of other research demonstrating active inhibition by ellagic acid,[35] quercetin,[36] and vitexin[37] against the α-amylase study. This was further supported *via* the binding pose, as displayed in Table S2 and Figures S4−S15 (Supporting Information). To gain an additional understanding of the behavior of bounded protein−ligand complexes, all of these compounds were run up to 100 ns MD simulation.

The MD simulation holds significant importance in the realm of pharmaceutical research due to its ability to offer valuable insights into the intricate behavior of molecules at both the atomic and molecular scales. This, in turn, enables researchers to acquire an in-depth comprehension of the interactions between these molecules and drug targets, thereby facilitating the optimization process.[38] Additionally, MD simulations can be used to estimate how long a ligand will remain attached to its target protein. Extended ligand-target residence durations are commonly linked with enhanced therapeutic effectiveness. Consequently, comprehending the dynamics of ligand association and dissociation is critical.[39] The structural behavior, molecular flexibility, and stability of α-amylase with various phytochemicals were accessed by a 100 ns MD simulation using GROMACS 2021.4. To comprehend the molecular dynamic results, several built-in GROMACS techniques such as RMSD, RMSF, SASA, radius of gyration, and hydrogen-bond analysis were performed.

2.3.1. Root-Mean-Square Deviation (RMSD). An assessment of RMSD evaluation was conducted to monitor the conformational and structural alterations of the atoms in the backbone of the enzyme−substrate and α-amylase complexes. The RMSD plot of α-amylase and all protein−ligand complexes was analyzed based on a 100 ns trajectory (Figure 1). It is noteworthy to mention that, except for ellagic acid, epicatechin, and protocatechuic acid, all protein−ligand complexes, as well as the apoprotein, achieved stability within a simulation time of 20 ns. The apoprotein was stable up to 80 ns, after which it showed slight fluctuation along with an average RMSD of 0.243 nm. The higher stability of the apigenin and caffeic acid complexes can be attributed to the fact that their RMSD values were within acceptable bounds (below 0.24 nm) compared to the apoprotein. The compounds kaempferol, quercetin, scutellarin, and vitexin achieved stability within 10 ns, exhibiting average RMSDs of 0.263, 0.270, 0.254, and 0.26 nm, respectively (Table 2). The acarbose−protein complex exhibited the highest level of stability, as evidenced by the RMSD value of 0.168 nm, also supported by prior studies.[40] This finding implies that the protein experienced less deviation upon formation of the complex with acarbose. Except

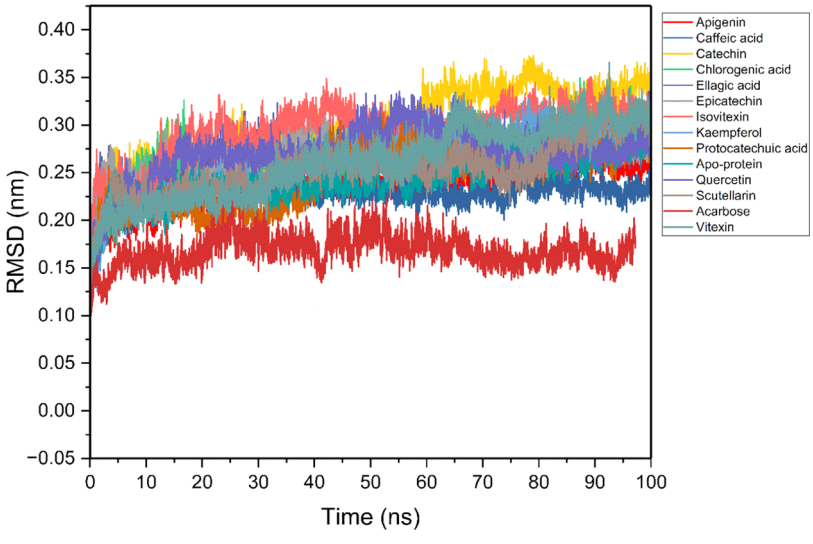

Figure 1. RMSD plot of the protein (α-amylase) and ligand (screened metabolites) complex.

https://doi.org/10.1021/acsomega.3c05082
ACS Omega 2023, 8, 43617−43631

Table 2. Average RMSD, R_g, RMSF, and SASA Value of Protein and Screened Ligands Complexes

complex	average RMSD (nm)	average R_g (nm)	average RMSF (nm)	average SASA (nm^2)
apoprotein	0.243	2.278	0.115	248.909
α-amylase–apigenin	0.235	2.256	0.102	250.017
α-amylase–caffeic acid	0.228	2.278	0.111	251.856
α-amylase–catechin	0.297	2.247	0.129	247.583
α-amylase–chlorogenic acid	0.272	2.263	0.111	246.769
α-amylase–ellagic acid	0.263	2.260	0.109	251.130
α-amylase–epicatechin	0.268	2.270	0.121	248.927
α-amylase–isovitexin	0.294	2.288	0.121	246.366
α-amylase–kaempferol	0.263	2.262	0.115	251.947
α-amylase–protocatechuic acid	0.247	2.266	0.128	251.945
α-amylase–quercetin	0.270	2.268	0.122	246.973
α-amylase–scutellarin	0.254	2.269	0.118	248.046
α-amylase–acarbose	0.168	2.369	0.0771	269.877
α-amylase–vitexin	0.26	2.275	0.129	248.433

for protocatechuic acid, all other protein–ligand complexes showed stability under a 100 ns simulation.

2.3.2. Radius of Gyration (R_g). The parameter radius of gyration (R_g) is utilized to assess the stability of both apoproteins and protein–ligand complexes during a 100 ns simulation. To assess the structural compactness, stability, and conformational states of the biomolecules, the R_g value was analyzed through the utilization of a molecular dynamics (MD) simulation trajectory.[41] The graph illustrating the variation of R_g over time for both apoprotein and protein–ligand complexes within a 100 ns time frame is presented in Figure 2.

The apoprotein α-amylase exhibited an average R_g of 2.278 nm, slightly lower than the previously reported value.[42] Except for the complexes involving α-amylase–acarbose, α-amylase-isovitexin, and α-amylase–caffeic acid, the remaining complexes exhibited reduced R_g values in comparison to the apoprotein. This suggests a more condensed structure in these complexes. The complex formed between α-amylase and catechin exhibited the lowest R_g value, specifically measuring 2.247 nm, whereas the α-amylase–acarbose complex displayed the highest R_g value, i.e., 2.369 nm. When compared to apoprotein, all of the compounds displayed relatively similar and consistent R_g values (Table 2). Throughout the 100 ns simulation, the acquired R_g value indicates the fact that all of the protein–ligand complexes attained a comparatively stable folded conformation. The α-amylase–acarbose complex displayed the highest radius of gyration, indicating that acarbose does not effectively fit within the protein's binding pocket. All of the ligands form a stable interaction with the protein compared to the acarbose and have a more compact structure. The average R_g value of ellagic acid, epicatechin, quercetin, and acarbose is comparable with previously reported values.[41] The results demonstrated improved compactness and rigidity of protein–ligand complexes, indicating overall complex stability.

2.3.3. Root-Mean-Square Fluctuation (RMSF). The RMSF value is a quantitative measure employed to assess the variations occurring in the native protein residues and ligand atoms under specific temperature and pressure conditions. A greater RMSF value denotes a more flexible part of the structure such as turns and loops and, conversely, a lower RMSF value suggests the presence of a more stable secondary structure, such as helices and sheets.[41] The fluctuations noted in the residues of the apoprotein and protein–ligand complexes during 100 ns simulation have been plotted as a function of time and are displayed in Figure 3. Consistent variations and RMSF values were observed within the identical residues across all complexes. The average RMSF values for various complexes, including apoprotein, α-amylase–apigenin, α-amylase–caffeic acid, α-amylase–chlorogenic acid, α-amylase–ellagic acid, and α-amylase–epicatechin, were determined to be 0.115, 0.102, 0.111, 0.129, 0.111, 0.109, and 0.121 nm,

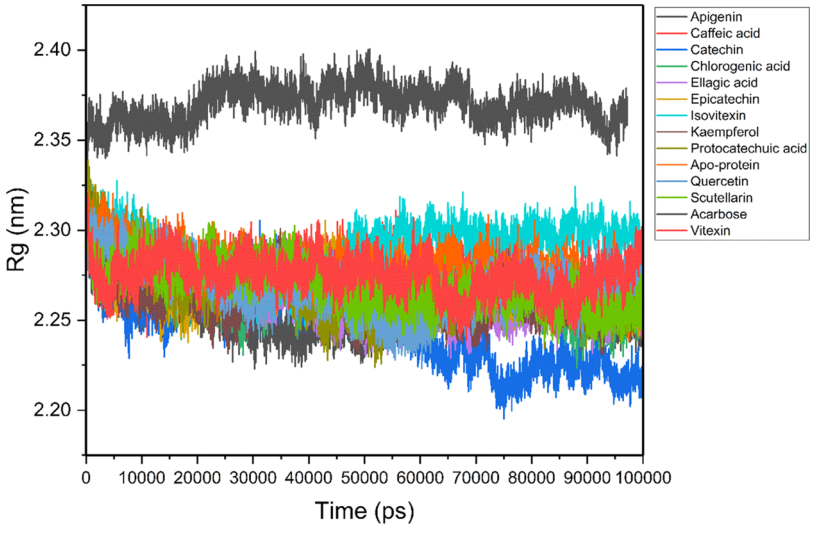

Figure 2. R_g plot of the protein (α-amylase) and ligand (screened metabolites) complex.

https://doi.org/10.1021/acsomega.3c05082
ACS Omega 2023, 8, 43617−43631

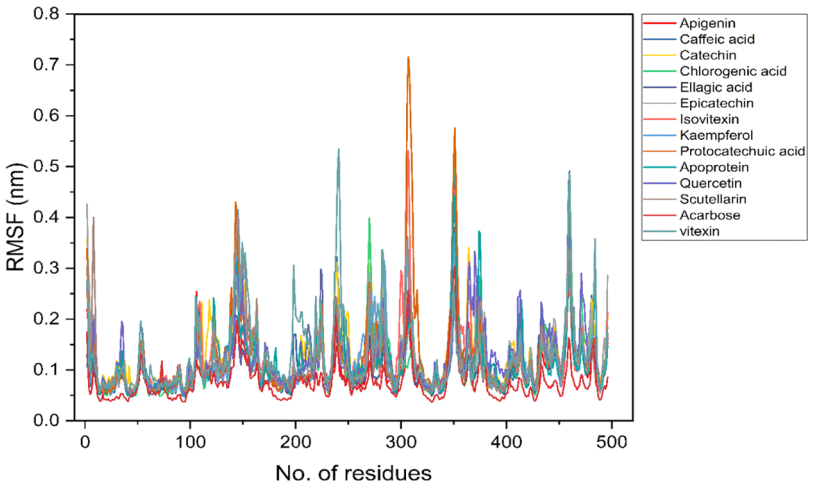

Figure 3. RMSF plot of the protein (α-amylase) and ligand (screened metabolites) complex.

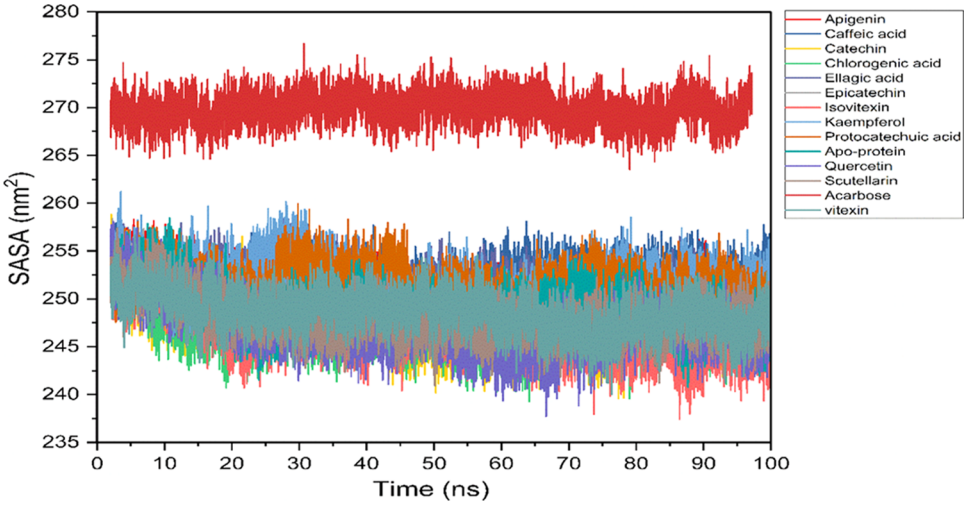

Figure 4. SASA plot of the protein (α-amylase) and ligand (screened metabolites) complex.

respectively. The average RMSF values for the complexes of α-amylase with isovitexin, kaempferol, protocatechuic acid, quercetin, scutellarin, acarbose, and vitexin were observed to be 0.121, 0.115, 0.128, 0.122, 0.118, 0.071, and 0.129 nm, respectively (Table 2).

RMSF results showed fluctuations of around 0.445, 0.438, 0.317, 0.369, 0.373, and 0.323 nm in residues ASN350, GLY351, ASN352, PRO374, ASP375, and GLY460, respectively, in apoprotein, consistent with a prior study.[42] Out of the selected protein−ligand complexes, α-amylase−protocatechuic acid showed the highest fluctuations compared to other complexes. Generally, the highest fluctuations were observed in residues LYS142, THR143, GLY144, GLU239, HIS305, GLY306, ALA307, GLY308, GLY309, ALA310, SER311, GLN349, ASN350, GLY351, PRO374, ASP375, and GLY460, which are not part of the active site. Both isovitexin and vitexin complexes showed almost similar types of fluctuations, which is also supported by a previous study.[43] From this result, we can conclude that except for α-amylase−protocatechuic acid complexes, all other protein−ligand complexes exhibited acceptable fluctuations and hence act as potent inhibitors of α-amylase.

2.3.4. Solvent-Accessible Surface Area (SASA). Solvent-accessible surface area (SASA) quantifies the proportions that comprise a biomolecule's surface area available for solvent interaction. Nevertheless, it also predicts the conformational changes during the interaction. The study determined the average SASA value of the apoprotein as 248.909 nm^2, while that of protein−ligand complexes ranged from 246 to 269 nm^2 (Table 2). Out of the selected complexes, catechin, chlorogenic acid, isovitexin, quercetin, scutellarin, and vitexin exhibited lower SASA values compared to that of apoprotein, implying effective binding interaction of these compounds within the binding pocket of the enzyme and thus resulting in a more compact complex (Figure 4). The α-amylase−isovitexin complex showed the lowest SASA value (246.366 nm^2), whereas the α-amylase−acarbose complex exhibited the highest SASA value (269.877 nm^2). The average SASA values of α-amylase−ellagic acid, α-amylase−epicatechin, and α-amylase−quercetin were found to be 251.130 nm^2, 248.927 nm^2, and 246.973 nm^2, respectively, lower than the previously reported value with HPA (PDB ID: 3BAJ).[41] The lower the SASA value, the more strongly the ligand can be accommodated within the catalytic site of the protein, and a more compact structure will be formed.[44] Since the SASA values of all of the complexes were analogous to those of the apoprotein, we can conclude that the selected phytochemicals act as potential inhibitors.

https://doi.org/10.1021/acsomega.3c05082
ACS Omega 2023, 8, 43617−43631

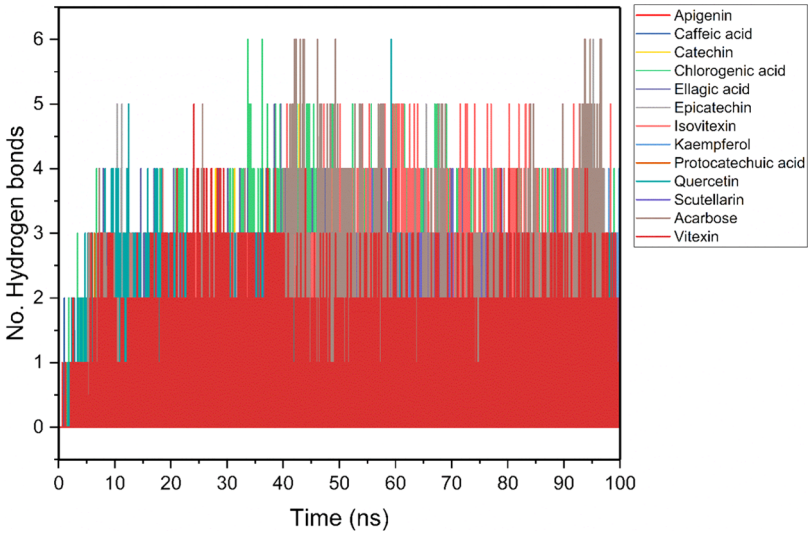

Figure 5. H-bond plot of the protein (α-amylase) and ligand (screened metabolites) complex.

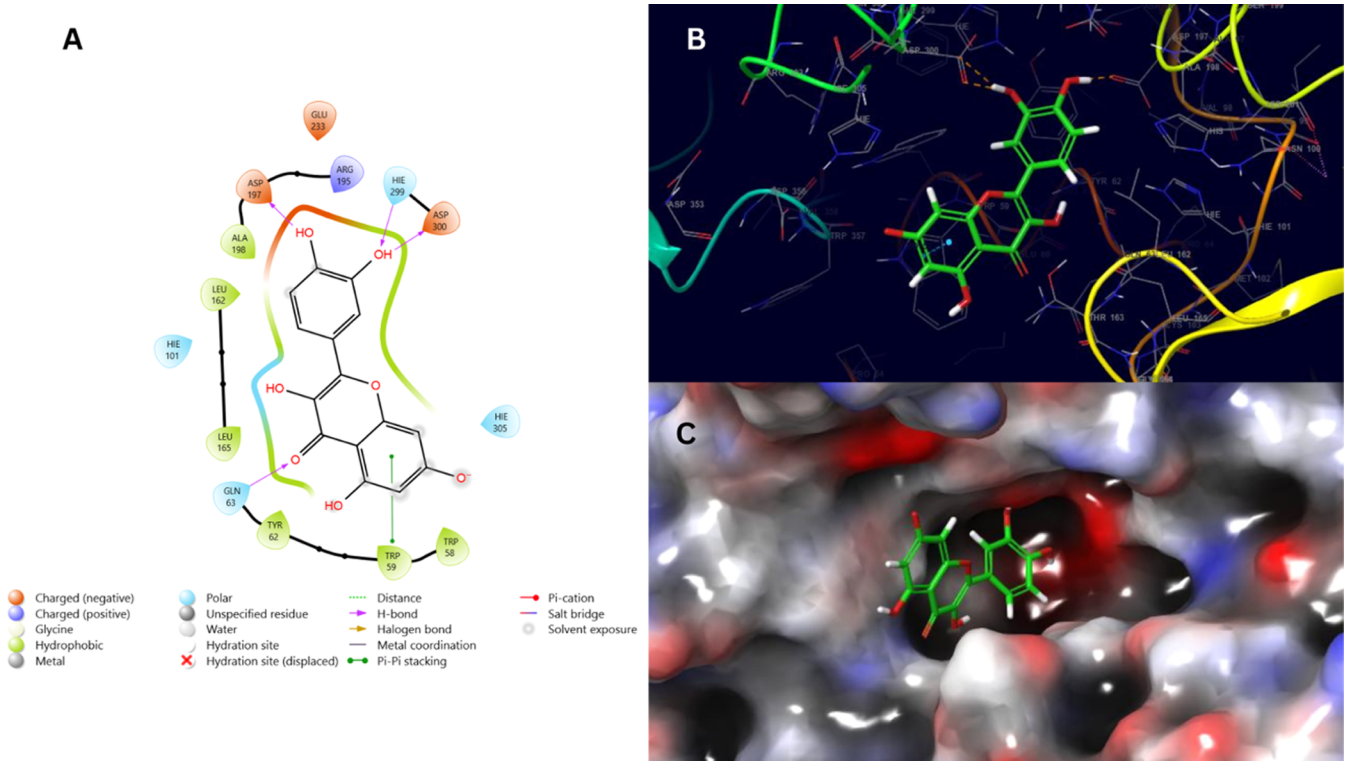

Figure 6. Molecular interaction and binding pose of quercetin in the binding site of HPA. (A) Two-dimensional (2D) ligand interaction, (B) three-dimensional (3D) interaction, and (C) molecular surface diagram of the quercetin−HPA complex.

2.3.5. Hydrogen Bonds. Considering the pivotal role of hydrogen bonds in facilitating substrate binding to proteins and their impact on various biological processes, such as metabolism, adsorption, drug affinity, and specificity, it becomes imperative to ascertain the hydrogen-bonding patterns by monitoring the dynamic fluctuations of hydrogen bonds across all protein−substrate complexes. It was noted that all of the complexes consistently maintained hydrogen bonds throughout the entire 100 ns simulation trajectory. In the complexes, α-amylase−epicatechin, α-amylase−isovitexin, α-amylase−quercetin, and α-amylase−vitexin complexes exhibited the six strongest hydrogen bonds (Figure 5). These observed hydrogen-bond results showed that all of the substrates were successfully and tightly bound to enzymes *via* hydrogen bonding.

The compounds protocatechuic acid, chlorogenic acid, and caffeic acid that showed weak interaction and low binding score exhibited high fluctuations, deviation, and SASA value along with less hydrogen-bonding interaction. Moderate simulation results were reported for apigenin, ellagic acid, kaempferol, scutellarin, and catechin. Although ellagic acid exhibited a prominent MM/GBSA value (−23.89 kcal/mol), it has the highest R_g and SASA value compared to other ligands, which suggests ellagic acid does not bind effectively in the

https://doi.org/10.1021/acsomega.3c05082
ACS Omega 2023, 8, 43617−43631

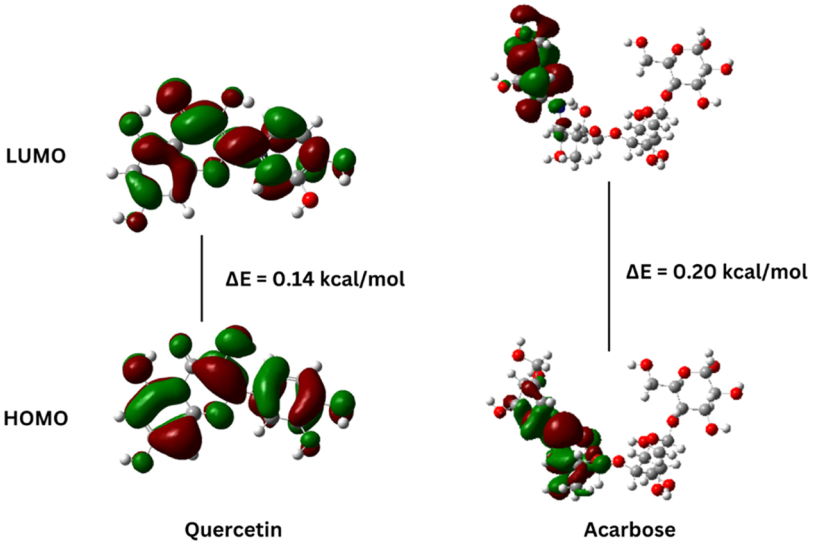

Figure 7. Band-gap energy illustration of quercetin and acarbose (standard).

binding pocket of the protein and forms less hydrogen bonding. Similarly, MD simulation results revealed epicatechin, isovitexin, quercetin, and vitexin exhibited up to six hydrogen bonds during 100 ns simulation. However, epicatechin, isovitexin, and vitexin were found to be bonded with only one catalytic site: GLU233, ASP197, and ASP300, respectively, and exhibited lower MM/GBSA binding scores as compared to the standard acarbose.

In context to both molecular docking and MD simulation, quercetin, the flavonoid metabolite, showed the most prominent binding interaction with the catalytic site residue as well as exhibited a prominent binding score and stable simulation results too. Using MM/GBSA, the most prominent binding score,[45,46] it was determined that quercetin (the only compound from the selected library of metabolites) showed a greater MM/GBSA of −27.03 kcal/mol in contrast to the standard drug acarbose (−26.69 kcal/mol). With regard to the binding pose, GLN63, ASP197, HIE299, and ASP300 amino acid residues, which are some of the binding site residues predicted by SiteMap, were found to be bonded with the quercetin metabolite *via* H-bonding, TRP59 by Pi−Pi stacking. Some similar binding interactions of quercetin were observed with the α-amylase enzyme (PDB ID: 3BAJ).[41] ASP197 and ASP300, being the two catalytic triad residues involved in the hydrolysis of dietary starch, are bonded with quercetin (Figure 6). According to the results of fluorescence quenching and enzyme activity, quercetin showed similar inhibitory actions against α-amylase activity through hydrogen and hydrophobic binding, further supported by fluorescence spectroscopy.[47] These findings suggest that quercetin has a greater affinity for binding than acarbose and might be potentially explored as a therapeutic agent. Furthermore, the molecular dynamics simulation supports the docking results. The RMSD, a crucial parameter used to determine the deviation in the skeleton of the protein after forming the complex, showed that the quercetin−α-amylase complex and apoprotein are almost equally stable. Similarly, the R_g and SASA values showed that quercetin−α-amylase is more compact compared to the apoprotein, indicating that quercetin binds strongly within the binding region (active site) of the protein and forms a compact structure. On the contrary, quercetin also maintains hydrogen bonding with the protein under 100 ns simulation. Overall, simulation results showed the stable quercetin−HPA complex in the context of the biological system and therefore illustrated its efficacy as a therapeutic inhibitor. This finding is consistent with the study that remarked quercetin exhibits stable 100 ns MD simulation results against HPA.[36,48]

2.4. DFT and Band-Gap Energy. An in-depth study using the DFT method was conducted to evaluate the reactivity of phytochemicals within the binding pocket of HPA. The energy levels of frontier molecular orbitals (FMOs) and band-gap energy ($E_{LUMO} - E_{HOMO}$) are key quantum parameters that significantly contribute to characterizing a molecule's interactions with other species, such as protein−ligand or ligand−ligand interactions.[49] Molecules with a lower band-gap energy tend to exhibit greater polarizability and higher chemical reactivity.[50] In addition, quantum molecular descriptors such as chemical potential (μ), global hardness (η), softness (s), and electrophilicity index (ω) are employed to elucidate the relationship between the protein−ligand and drug efficacy in systems used for drug delivery. The Pearson principle of maximum hardness states that the chemical hardness inversely affects reactivity. Compounds with reduced chemical hardness and higher softness are considered to be more reactive.[51] A higher electronegativity (χ), electrophilicity indices, and chemical potentials correspond to a greater chemical reactivity with catalytic proteins as they serve as good electrophiles rather than nucleophiles.[52] Similarly, the electrophilicity index (ω) quantifies a molecule's electron-accepting capacity and the chemical potential (μ) indicates the path of electron transfer.

Following molecular docking, MD simulation, and MM/GBSA binding energy calculations, quercetin was selected for the DFT analysis. The standard compound, acarbose, was also considered to compare the reactivity with that of quercetin. The optimal geometric structures of the hit molecule under study are shown in Figure S16 (Supporting Information).

The result demonstrated that quercetin has effective reactivity due to the low band gaps of HOMO and LUMO (0.14 kcal/mol) relative to the standard compound acarbose (0.20 kcal/mol) (Figure 7). Due to the C2═C3 double bond in the C ring, quercetin, the greatest antioxidant, exhibited the highest HOMO energy value, a planar structure, and the best electron orbital delocalization on all phenolic rings.[53] Moreover, the quantum mechanical parameters such as η, S, χ, μ,

https://doi.org/10.1021/acsomega.3c05082
ACS Omega 2023, 8, 43617−43631

and ω that are concerned with the reactivity suggest the high potency of quercetin toward HPA (Supporting Information, Table S3).

The study generated MEP maps of the analyzed compounds to ascertain the electron-rich and -deficient regions within the compound. The MEP map is presented with a chromatic scheme as displayed in Figure 8. The blue coloration in the diagram represents the positive region, which is associated with a nucleophilic attack. Conversely, the red coloration indicates a negative region, which is indicative of an electrophilic attack. The green coloration, on the other hand, represents areas of zero potential within the molecule.[54]

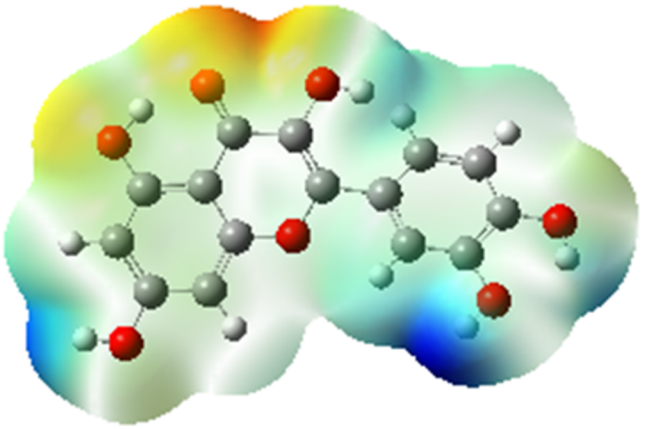

Figure 8. MEP map of quercetin.

The study revealed that oxygen atoms exhibited negative charges, whereas hydrogen atoms that formed bonds with oxygen or nitrogen atoms exhibited positive charges. The negative and positive centers played a crucial role in the establishment of noncovalent interactions between ligands and receptors throughout molecular docking and MD simulations.[55] Accordingly, the blue region in the MEP map, which depicts the electron-deficient center, entails hydrogen bonding between two hydrogens of hydroxyl groups of ring B on quercetin (hydrogen donor) and ASP300, ASP197, and HIS299 residues of HPA (hydrogen acceptor) as illustrated in Figures 6 and 9. Similarly, the red region of the diagram, which denotes the negative electrostatic potential, acts as a hydrogen-bond acceptor where the GLN63 HPA residue interacts with the electron-rich carbonyl group of quercetin. This study, therefore, encloses the molecular interactions and binding patterns between quercetin and HPA aiding in the docking and simulation results.

2.5. Pharmacokinetic Analysis. To be a drug, a candidate needs to be extremely selective and possess low undesirable effects.[56] Drug candidates often experience a notable attrition rate during the later stages of development, primarily due to their efficacy and the unavoidable occurrence of adverse effects, which are largely attributed to ADMET issues.[57] However, the potential failure of a promising candidate can be minimized by employing an *in silico* technique. As a result, the drug-likeness and ADMET properties of the potential hit

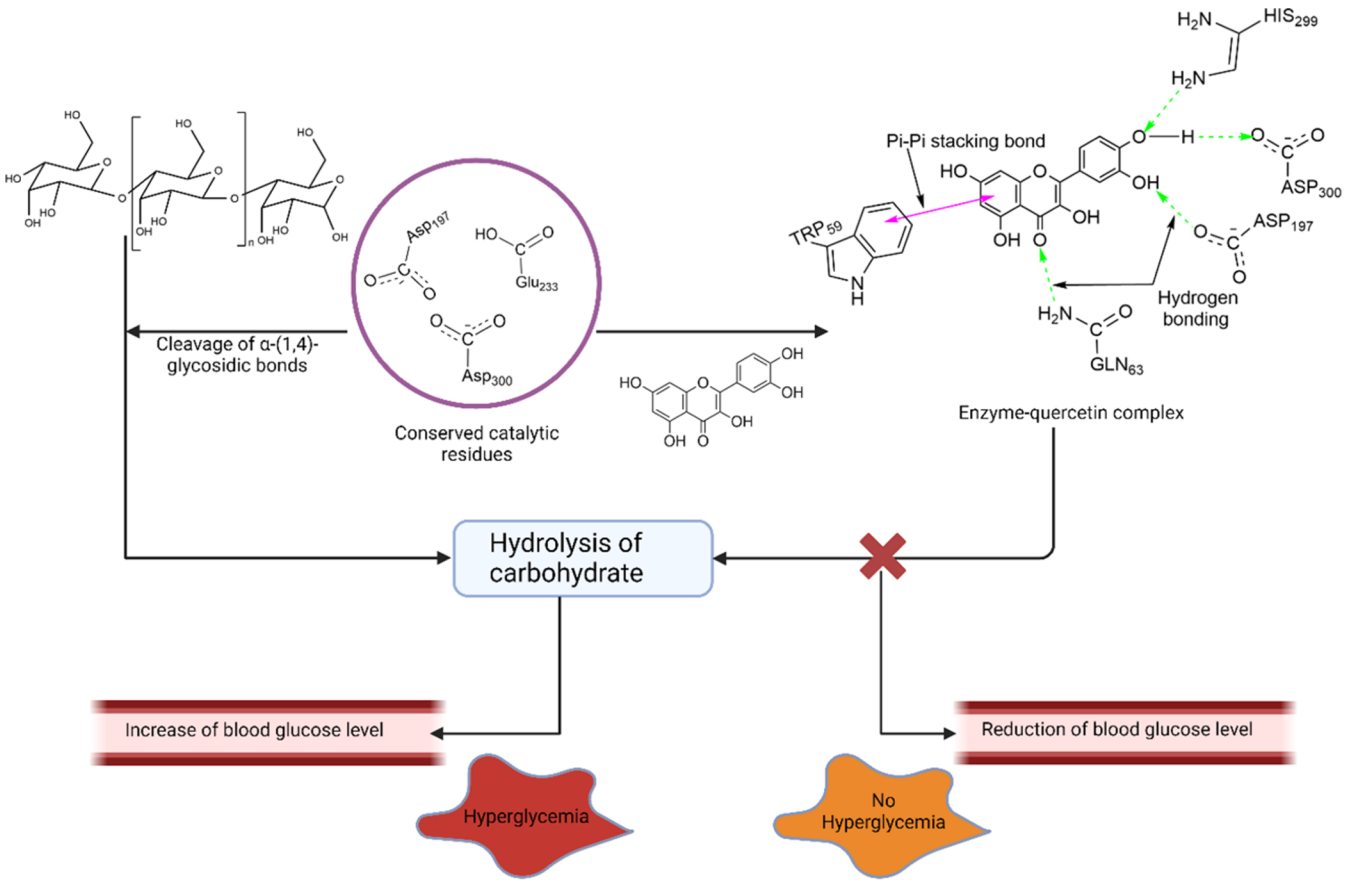

Figure 9. Mechanism of quercetin in the inhibition of HPA.

https://doi.org/10.1021/acsomega.3c05082
ACS Omega 2023, 8, 43617−43631

Table 3. Drug-Likeness Properties of Quercetin and Acarbose *via* the SwissADME Server

	no. of rotatable bonds	no. of H-bond acceptors	no. of H-bond donors	TPSA (Å)	MLOGP	molar refractivity	Lipinski's rule of five	Ghose filter	Veber rule	Egan rule	drug-likeness
quercetin	1	7	5	131.36	− 0.56	78.03	yes; 0 violation	yes	yes	yes	accepted
acarbose	9	19	14	321.17	− 6.94	136.69	no; 3 violations	no; 4 violations	no; 1 violations	no; 1 violations	rejected

(quercetin) were thoroughly examined employing several models, including QikProp, SwissADME, admetSAR, and pkCSM (Table 3, Supporting Information S4−S6).

For any compound to be a potent drug candidate, it should be easily absorbed in the body. The hit compound showed that 77.207% intestinal absorption surpasses the minimal absorption criteria of 30%[58] and is much greater than the acarbose value (4.172%). The log VDss and blood−brain barrier (BBB) permeability signifying tissue distribution and accumulation into the brain leading to neurotoxicity,[59] respectively, have revealed the hit compound quercetin to be safer in this perspective. Quercetin's neuroprotective benefits have been corroborated by several investigations conducted *in vitro*, *in vivo*, and in humans. Low concentrations of quercetin (from picomolar to nanomolar) are discovered in the brain tissue of rats and pigs after quercetin is administered *in vivo* successfully attempting to improve quercetin's bioavailability.[60,61] Cytochrome P450 enzymes (key CYP3A4) contribute significantly to the detoxification of foreign chemicals and help in the metabolism of drugs.[62] The hit compound does not inhibit CYP3A4, indicating it is easily metabolized in the liver and has no side effects. The organic-anion-transporting polypeptide 1B1 (OATP1B1/SLCO1B1) transporter is a prominently expressed uptake transporter in the human liver. Its significance lies in its crucial role in drug disposition. OATP1B1, OATP1B3, and the less widely recognized OATP2B1 (SLCO2B1) are all expressed in the basolateral membrane of hepatocytes and play a crucial role in mediating the transport of xenobiotics and endogenous compounds from the portal circulation.[63] The hit compound showed the OATP1B1 substrate of the phosphate−OATP1B1 complex, leading to a decrease in potential side effects and toxicity. As of a previous study conducted on Chinese-Han males, quercetin inhibits OATP1B1 substrates with a modest inhibitory pravastatin pharmacokinetic impact on healthy volunteers.[64] Hepatotoxicity and AMES toxicity are key factors determining liver injury and mutagenicity caused by the drugs.[65] Quercetin showed both negative AMES toxicity tests and hepatotoxicity. It thus aligns with the conclusion that quercetin is not a CYP3A4 inhibitor, is not toxic to the liver, and has no AMES toxicity.[66]

To assess the possibility of assay interference or toxicity, the quantification of reactive functional groups (#rtvFG) present in each molecule was also evaluated and found to be within the range. Further, it was observed that both quercetin and acarbose showed CNS inactive properties. SASA value, which indicates the free surface area of the molecule, was also within the acceptable range. Since cell membranes are lipoid, the hit compound's lipophilicity (QPlog $P_{o/w}$) of 0.362 (−2.0 to 6.5) suggests it is less hydrophilic and may be readily absorbed and dispersed inside cells. The presence of the hydroxyl group may account for the compound's hydrophilic nature, while the presence of both the aromatic ring and the keto-functional group may account for its lipophilic nature.[67] Similarly, the ADMET properties of the hit compound were also evaluated in terms of QPlogHERG (predicted IC_{50} values for the blockage of human ether-a-go-go-related gene potassium ion channels), QPlogBB (predicted brain−blood partition coefficient), QPlogkhsa (prediction of binding to human serum albumin), and #metab (number of likely metabolic reactions). Consistent with an earlier study,[68] the hit compound possessed a blood−brain partition coefficient and QPlogHERG within the acceptable range alongside its binding with human serum albumin. The Qikprop ADMET results showed quercetin (hit compound) has better pharmacological properties compared to acarbose. The reported ADME properties of quercetin, as well as its tolerable oral toxicity, decreased rat oral toxicology, in addition to the noncarcinogenic or mutagenic potential,[69] further supporting our result.

Quercetin was further subjected to Lipinski's (Pfizer) rule of 5, the Ghose Filter, Veber's rule, and the Egan rule to predict whether the compound under study has a drug-like property or not. With a molecular weight of 302.24 g/mol, −0.56 log *P*, five hydrogen-bond donors, and seven hydrogen-bond acceptors, quercetin showed zero violation in Lipinski's rule, demonstrating a drug-likeness property. The Ghose Filter, another parameter sought to evaluate the drug-likeness of compounds, relies on the evaluation of various physicochemical properties, including log *P* values (−0.4 to 5.6), molar refractivity values (40−130), molecular weight (160−480), number of atoms (20−70), and topological polar surface area (TPSA) ≤ 140 Å^2.[70] Quercetin followed Ghose's rule with its acceptable aforementioned range. Since the investigated compound has no more than 140 Å^2 TPSA and 10 rotatable bonds, it meets the criteria of Veber's rule.[71] TPSA is the parameter to evaluate the competence of the drug to permeate cells: TPSA > 140 Å^2 and rotatable bond > 10 denote poor permeability of drugs.[72] The Egan rule states that a candidate drug has good oral absorption if − 1.0 ≤ log *P* ≤ 5.8 and TPSA ≤ 130 Å^2;[73] quercetin was found to follow this rule within acceptable log *P* and TPSA values. These results indicate that no violations were observed for quercetin in terms of the Lipinksi, Ghose, Veber, and Egan rules, whereas acarbose, the reference compound, demonstrated noncompliance with all of these drug-likeness parameters. The finding is further supported by earlier research showing quercetin to be a drug-like candidate that satisfies all of the aforementioned criteria.[66] Additionally, the number of stars evaluated *via* Qikprop indicates the drug-likeness properties of molecules, where higher numbers of stars indicate less drug-likeness properties.[74] The #stars result showed quercetin has better drug-likeness properties compared to acarbose.

2.6. α-Amylase Inhibition Assay. During the enzyme assay, quercetin was found to inhibit pancreatic α-amylase with an IC_{50} value of 57.37 ± 0.9 μg/mL, which is almost comparable with that of the standard compound, acarbose (53.9 ± 0.3 μg/mL) (Supporting Information, Figure S17 and Table S7). This observed inhibition result aligns with the

https://doi.org/10.1021/acsomega.3c05082
ACS Omega 2023, 8, 43617−43631

findings reported in the existing literature, which indicate that quercetin can inhibit PPA.[26,48,75] PPA and HPA are substantially comparable in terms of their three-dimensional structures. Molecular cloning and primary structural analysis of PPA revealed that it shared the highest similarity to the HPA sequence of all known amylases (87.1%).[76] Consequently, it is postulated that quercetin may exert a beneficial inhibitory effect on HPA as well. Therefore, the findings suggest that quercetin, the compound anticipated through computational methodology, possesses the capacity to impede the pancreatic α-amylase, thereby diminishing the breakdown of carbohydrates into maltose.

It is worth noting that the exact mechanism of quercetin's α-amylase inhibition may vary depending on the specific enzyme and experimental conditions. Quercetin exhibits competitive binding to the active site of α-amylase, effectively impeding the enzyme's ability to engage with its substrate, starch. This inhibition occurs through the disruption of noncovalent interactions, including hydrogen bonding and hydrophobic interactions.[77] In accordance with our study, depicted in Figure 9, quercetin, the hit flavonoid, forms hydrogen bonding with the catalytic triad (ASP197, GLU233, and ASP300) and inhibits the hydrolysis reaction. Some studies have suggested that quercetin may also inhibit α-amylase through noncompetitive or mixed inhibition, where it binds to sites other than the active site, thereby affecting the enzyme function indirectly.[47] Besides these, quercetin has been found to enhance plasma insulin levels and reduce blood glucose levels in diabetes models induced by streptozotocin (STZ) *via* preservation of β-cell mass and function, ultimately leading to an increase in the serum insulin efficacy. Moreover, a study concluded that quercetin exhibited the ability to mitigate islet cell dysfunction, enhance β-cell insulin secretion, and forestall diabetes by diminishing oxidative stress in alloxan-induced diabetic animal models.[78]

Quercetin, a bioflavonoid, is a plant pigment that is found in over 20 different plant materials and is well-known for its therapeutic biological activities including antiobesity, antihypertensive, antihypercholesterolemic, anticancer, antibacterial, antiatherosclerotic activities, antiviral, and so on.[79−81] Since quercetin is a dietary flavonoid distributed in various food sources such as fruits (particularly citrus, apples, and cherries), vegetables (onions, broccoli), and beverages (tea and red wine)[82] and is granted Generally Recognized as Safe (GRAS) status to quercetin (QU995) by the Food and Drug Administration (FDA), its consumption might be beneficial in terms of diabetes and other aforementioned diseases. Moreover, oxidative stress (OS), together with insulin insufficiency, leads to T2D;[83] OS arises from the production of free radicals and reactive oxygen species (ROS), which disrupt the body's protective mechanisms. Consequently, T2D manifests as a consequence of elevated levels of ROS.[84] Consuming dietary sources of quercetin, which are rich in antioxidants and can decrease carbohydrate consumption *via* α-amylase inhibition, would be an attractive strategy for combating hyperglycemia, particularly T2D.

The clinical utility of quercetin, classified as a BCS class II drug, is impeded by numerous factors, encompassing its insufficient solubility in aqueous solutions, restricted permeability, a vulnerability in physiological milieus such as the gastric and intestinal tracts, transient biological half-life, and a substantial hepatic metabolism prior to systemic dissemination.[85] The combined influence of these factors contributes to the less-than-ideal oral bioavailability of quercetin, thus imposing restrictions on its use in pharmaceutical utilization. Nevertheless, novel methodologies have been previously documented in the literature to address this issue, encompassing the development of solid lipid nanoparticles, self-nano emulsifying systems, polymeric nanoparticles, liposomes, nanocrystals, and cationic nanocarriers to augment the bioavailability of quercetin, thereby exemplifying a favorable inclination toward the clinical phase of quercetin.[86]

3. CONCLUSIONS

Inhibition of HPA has been a strategic approach to suppress carbohydrate digestion, resulting in a reduced rate of glucose release into the bloodstream and thereby controlling T2D and its associated complications. Polyphenols, which make up a heterogeneous group of secondary metabolites present in diverse plant species and dietary sources, have emerged as the subject of considerable study in recent times attributable to their potential health-promoting properties, particularly their capacity to regulate hyperglycemia. Based on the molecular docking and MD simulation of 12 secondary metabolites, our findings suggest that quercetin exhibits potential as a viable candidate. This is attributed to its MM/GBSA value, which surpasses that of acarbose, as well as its ability to interact with catalytic site residues, thereby inhibiting the hydrolysis of glycosidic bonds present in carbohydrates and ultimately controlling hyperglycemia. Additionally, quercetin demonstrated significant stability with HPA, as evidenced by its RMSD, RMSF, R_g, SASA, and H-bonding properties, further highlighting its efficacy within biological systems. The DFT analysis indicates that quercetin, in comparison to the reference compound acarbose, has a high reactivity in the binding pocket of HPA. After this, an evaluation of the pharmacokinetic parameters, encompassing the ADMET analysis, and the drug-likeness properties provides additional substantiation for its potential as a pharmaceutical candidate, and to determine its efficacy, an *in vitro* pancreatic α-amylase inhibition assay was conducted. The computational study was corroborated by the IC_{50} value of 57.37 ± 0.9 μg/mL, thereby inferring quercetin as a potent HPA inhibitory agent. Although quercetin has been documented as a significant metabolite in diverse ailments, it has not yet been contemplated for clinical trials in the administration of diabetes. The recorded consequences and revelations of *in vitro* exploration produced advantageous outcomes in conjunction with our computational evaluation. Hence, it is crucial to emphasize the importance of quercetin in forthcoming research undertakings, which ought to encompass *in vivo* models and headway toward sophisticated phases of drug investigation plans.

4. MATERIALS AND METHODOLOGY

4.1. Selection and Preparation of Ligands. With the purpose of screening for potential HPA inhibitors, a library of 12 phenolic secondary metabolites based on their biological properties was generated (Supporting Information, Figure S18 and Table S8), along with acarbose, which is a standard compound employed for diabetes treatment. Using the PubChem database (https://pubchem.ncbi.nlm.nih.gov), the 3D conformers of each ligand were retrieved in SDF (structure data format). Each of the ligand structures was imported into Maestro's workspace using Schrödinger's LigPrep module, and subsequently, the energy was optimized employing the OPLS4

https://doi.org/10.1021/acsomega.3c05082
ACS Omega 2023, 8, 43617−43631

force field.[87,88] Additionally, Epik effectively generated tautomeric and ionization states while maintaining the specified chiralities at pH 7.0 ± 2.0 and generated up to 32 conformers per ligand into the maestro output format.

4.2. Protein Preparation. The HPA protein (PDB ID: 1HNY) of 1.80 Å resolution and zero mutation was retrieved from the Research Collaboratory for Structural Bioinformatics (RCSB) Protein Data Bank (https://www.rcsb.org/), and the protein preparation workflow was conducted following Schrödinger's methodology.[89] The CCD database was used to assign bond order, hydrogens were replaced, and zero-order bonds were formed between metals and disulfides as part of the preprocessing. Using glide, processes like filling in missing loops and filling in missing chains were carried out. The het states were subsequently generated with Epik under controlled conditions at a pH of 7.0 ± 2.0.[90,91] The hydrogen bonds were optimized through the application of PROPKA and subjected to minimization employing the OPLS4 force field[24] alongside the deletion of water with a distance of 5 Å from the ligands. The SiteMap application evaluated and validated the generated protein's quality and its ligand binding site.[24] ASP197, GLU233, and ASP300, which are catalytic triad residues, were incorporated into the protein to generate a receptor grid *via* a receptor grid generation program.

4.3. Molecular Docking. With regard to the Schrödinger glide module for ligand docking, Schrodinger (Release 2023-02) was utilized. The molecular docking of secondary metabolites with HPA was accomplished using the Glide software in its extra precision mode (XP).[92] The docking procedure was validated using redocking approaches and superimposition to ensure the precision and consistency of docking while also attempting to minimize misleading-positive outcomes.[93]

4.4. MM/GBSA Binding Energy Calculation. The MM/GBSA binding energy of protein−ligand complexes was assessed through the employment of Schrödinger's prime module.[90] An OPLS4 force field and the implicit VSGB solvation model[94] were utilized to determine the binding energy.

4.5. Molecular Dynamic Simulation. A molecular dynamic (MD) simulation of 100 ns was performed to study the stability, H-bonding between the ligand and the protein, and the dynamic protein−ligand complex behavior.[95] Gromacs software, version 2021.4, was used for performing MD simulations.[96] Initially, the protein's topology file was created using the GROMOS43a1 force field, and the PRODRG web server (https://www.sites.google.com/site/vanaaltenlab/prodrg) was used to create the ligand topology file.[97−99] Utilizing a rudimentary water model, the solvation of each protein−ligand complex was achieved within a triclinic box endowed with a stoichiometric intermolecular potential, thereby facilitating a spatial separation of at least 1.0 nm between the complex and each side of the three-dimensional enclosure.[100] The ionization state of the protein residues was determined according to their typical behavior under physiological conditions (pH 7.0) while periodic boundary conditions. The Monte-Carlo ion-placing method was employed to introduce the appropriate quantities of Na^+ and Cl^- ions to attain the overall neutrality of the entire complex.[101] Three steps were involved in the MD simulation. The first step comprised the initial optimization of each system's geometry using the steepest descent method over 5,000 iterations (5 ps). The subsequent procedure entailed employing the Berendsen temperature coupling technique to facilitate the initial equilibrium phase while maintaining constant particle number, volume, and temperature (NVT) conditions. The final equilibration step was conducted employing the Parrinello−Rahman barostat, which ensured the preservation of a consistent number of particles, pressure, and temperature throughout the entirety of the procedure.[102] Ultimately, molecular dynamics (MD) simulations were executed for a duration of 100 ns, employing the constant pressure (NPT ensemble) methodology.

4.6. Density Functional Theory (DFT) Analysis. The reactivity and effectiveness of phytochemicals against α-amylase were investigated using Gaussian 09 and Gaussview 6.0 software programs, employing density functional theory (DFT)-based analysis. The energy levels of the highest occupied molecular orbital (HOMO) and the lowest unoccupied molecular orbital (LUMO) were computed utilizing the 6-31G(d,p) basis set and the Becke, 3-parameter, Lee−Yang−Parr (B3LYP) correlation function of density functional theory (DFT).[103] The energy gap was determined by the subsequent equation[104]

$$\Delta E_{gap} = E_{LUMO} - E_{HOMO} \quad (1)$$

The given equation was employed to determine the ionization potential (IP), electron affinity (EA), as well as quantum mechanical parameters such as global hardness (η), global softness (S), electronegativity (χ), electrophilicity index (ω), and chemical potential (μ).[51,105]

$$IP = -E_{HOMO} \quad (2)$$

$$EA = -E_{LUMO} \quad (3)$$

$$\eta = \frac{\Delta E}{2} \quad (4)$$

$$S = \frac{1}{\eta} \quad (5)$$

$$\chi = \frac{(I + A)}{2} \approx -\mu \quad (6)$$

$$\omega = \frac{(\mu^2)}{2\eta} \quad (7)$$

The molecular electrostatic potential (MEP) diagram was used to explore the responsiveness of drug delivery systems to electrophilic or nucleophilic assaults and to depict the distribution of electron density.

4.7. Pharmacokinetic Analysis. The pharmacokinetic parameters of the hit molecule were assessed using ADMET analysis (absorption, distribution, metabolism, excretion, and toxicity) and drug-likeness properties. From the PubChem database, the canonical SMILES (Simplified Molecular Input Line Entry System) of the chosen compounds were extracted directly by copying and submitted to the appropriate servers for their respective analysis. The aforementioned parameters were accomplished using the admetSAR 2.0,[106] pkCSM web server,[107] and the SwissADME bioinformatics tool.[108] Similarly, Schrödinger's QikProp model was also considered, concerning ADME pharmacokinetic profiles of the optimal compound.

4.8. *In Vitro* Assays with α-Amylase. *4.8.1. Chemical and Materials.* Acarbose, porcine pancreatic α-amylase (PPA),

https://doi.org/10.1021/acsomega.3c05082
ACS Omega 2023, 8, 43617−43631

2-chloro-4-nitrophenyl-α-D-maltotrioside (CNPG3), and quercetin were purchased from the esteemed supplier Sigma-Aldrich (Germany). The acquisition of dimethyl sulfoxide and other required chemicals was facilitated by Fisher Scientific (India).

4.8.2. α-Amylase Inhibition Assay. The assessment of α-amylase inhibition was performed using a widely recognized methodology as outlined in the literature, with slight modifications.[109] A solution of quercetin (20 μL) in 5% DMSO was mixed with 80 μL of enzyme PPA (1.5 U/mL) in 50 mM phosphate-buffered saline (pH 7.0, 0.9% NaCl) and subjected to preincubation at 37 °C for 15 min. The enzymatic reaction was initiated through the addition of CNPG3 as the substrate at a concentration of 375 μM, followed by a 15 min incubation period at the same temperature, 37 °C. The absorbance measurement was performed using a microplate reader, specifically at a wavelength of 405 nm. The evaluation of inhibitory activity was ascertained using the following formula

$$\% \text{ inhibition} = \left(\frac{A_{\text{control}} - A_{\text{sample}}}{A_{\text{control}}}\right) \times 100$$

where A is the absorbance of the sample and the control.

■ ASSOCIATED CONTENT

Supporting Information

The Supporting Information is available free of charge at https://pubs.acs.org/doi/10.1021/acsomega.3c05082.

Binding site result predicted by SiteMap (Table S1); binding interaction and types of interaction of selected metabolites with HPA (Table S2); DFT result of selected metabolites against HPA (Table S3); ADMET properties of quercetin and acarbose obtained *via* QikProp (Table S4); ADMET properties of quercetin and acarbose *via* admetSAR 2.0 server (Table S5); ADMET properties obtained *via* the pkCSM web server (Table S6); IC_{50} value of quercetin and acarbose (Table S7); list of selected polyphenols and flavonoids (Table S8); ERRAT of HPA (PDB ID: 1HNY) (Figure S1); binding site of the protein predicted by SiteMap (Figure S2); superimposition of the cognate ligand into the active site of HPA (Figure S3); molecular interaction and binding pose of 11 selected metabolites and acarbose (standard) (Figures S4−S15); optimized structure of quercetin (Figure S16); α-amylase inhibition of quercetin and acarbose (standard) (Figure S17); structure of the selected metabolites (Figure S18) (PDF)

■ AUTHOR INFORMATION

Corresponding Author

Niranjan Parajuli − *Central Department of Chemistry, Tribhuvan University, Kirtipur 44600 Kathmandu, Nepal;* orcid.org/0000-0002-9233-6489; Email: niranjan.parajuli@cdc.tu.edu.np

Authors

Bimal K. Raut − *Central Department of Chemistry, Tribhuvan University, Kirtipur 44600 Kathmandu, Nepal*

Siddha Raj Upadhyaya − *Central Department of Chemistry, Tribhuvan University, Kirtipur 44600 Kathmandu, Nepal*

Jyoti Bashyal − *Central Department of Chemistry, Tribhuvan University, Kirtipur 44600 Kathmandu, Nepal*

Complete contact information is available at: https://pubs.acs.org/10.1021/acsomega.3c05082

Author Contributions

B.K.R and S.R.U. performed *in silico* and *in vitro* works and were involved in data analysis, J.B. drafted the manuscript, and N.P. revised the manuscript and supervised the project.

Notes

The authors declare no competing financial interest.

■ ACKNOWLEDGMENTS

The authors would like to acknowledge Schrodinger Inc. for the software license support.

■ ABBREVIATIONS

ADMET:Absorption, distribution, metabolism, excretion, and toxicity; B3LYP:Becke, 3-parameter, Lee−Yang−Parr; CNPG3:2-chloro-4-nitrophenyl-α-D-maltotrioside; DFT:density functional theory; DM:diabetes mellitus; DMSO:dimethyl sulfoxide; HOMO:highest occupied molecular orbital; HPA:-human pancreatic α-amylase; IC_{50}:half-maximal inhibitory concentration; LUMO:lowest unoccupied molecular orbital; MD:molecular dynamics; MM/GBSA:molecular mechanics with generalized Born and surface area solvation; PPA:porcine pancreatic lipase; R_g:radius of gyration; RMSD:root-mean-square deviation; RMSF:root-mean-square fluctuation; SASA:-solvent-accessible surface area; T2D:type II diabetes

■ REFERENCES

(1) Henrissat, B. A Classification of Glycosyl Hydrolases Based on Amino Acid Sequence Similarities. *Biochem. J.* **1991**, *280* (2), 309−316.

(2) Hall, F. F.; Ratliff, C. R.; Hayakawa, T.; Culp, T. W.; Hightower, N. C. Substrate Differentiation of Human Pancreatic and Salivary Alpha-Amylases. *Dig. Dis. Sci.* **1970**, *15* (11), 1031−1038.

(3) Saeedi, P.; Petersohn, I.; Salpea, P.; Malanda, B.; Karuranga, S.; Unwin, N.; Colagiuri, S.; Guariguata, L.; Motala, A. A.; Ogurtsova, K.; Shaw, J. E.; Bright, D.; Williams, R. Global and Regional Diabetes Prevalence Estimates for 2019 and Projections for 2030 and 2045: Results from the International Diabetes Federation Diabetes Atlas, 9th Edition. *Diabetes Res. Clin. Pract.* **2019**, *157*, No. 107843.

(4) Usai, R.; Majoni, S.; Rwere, F. Natural Products for the Treatment and Management of Diabetes Mellitus in Zimbabwe-a Review. *Front. Pharmacol.* **2022**, *13*, No. 980819.

(5) Liu, W.; Luo, Z.; Zhou, J.; Sun, B. Gut Microbiota and Antidiabetic Drugs: Perspectives of Personalized Treatment in Type 2 Diabetes Mellitus. *Front. Cell. Infect. Microbiol.* **2022**, *12*, No. 853771.

(6) Guarino, M.; Altomare, A.; Emerenziani, S.; Di Rosa, C.; Ribolsi, M.; Balestrieri, P.; Iovino, P.; Rocchi, G.; Cicala, M. Mechanisms of Action of Prebiotics and Their Effects on Gastro-Intestinal Disorders in Adults. *Nutrients* **2020**, *12* (4), 1037.

(7) Tan, K.; Tesar, C.; Wilton, R.; Jedrzejczak, R. P.; Joachimiak, A. Interaction of Antidiabetic A-glucosidase Inhibitors and Gut Bacteria A-glucosidase. *Protein Sci.* **2018**, *27* (8), 1498−1508.

(8) Brayer, G. D.; Luo, Y.; Withers, S. G. The Structure of Human Pancreatic α -Amylase at 1.8 Å Resolution and Comparisons with Related Enzymes. *Protein Sci.* **1995**, *4* (9), 1730−1742.

(9) Ferey-Roux, G.; Perrier, J.; Forest, E.; Marchis-Mouren, G.; Puigserver, A.; Santimone, M. The Human Pancreatic α-Amylase Isoforms: Isolation, Structural Studies and Kinetics of Inhibition by Acarbose. *Biochim. Biophys. Acta, Protein Struct. Mol. Enzymol.* **1998**, *1388* (1), 10−20.

(10) Rydberg, E. H.; Li, C.; Maurus, R.; Overall, C. M.; Brayer, G. D.; Withers, S. G. Mechanistic Analyses of Catalysis in Human Pancreatic α-Amylase: Detailed Kinetic and Structural Studies of Mutants of Three Conserved Carboxylic Acids. *Biochemistry* **2002**, *41* (13), 4492−4502.
(11) Ogunyemi, O. M.; Gyebi, G. A.; Saheed, A.; Paul, J.; Nwaneri-Chidozie, V.; Olorundare, O.; Adebayo, J.; Koketsu, M.; Aljarba, N.; Alkahtani, S.; Batiha, G. E.-S.; Olaiya, C. O. Inhibition Mechanism of Alpha-Amylase, a Diabetes Target, by a Steroidal Pregnane and Pregnane Glycosides Derived from Gongronema Latifolium Benth. *Front. Mol. Biosci.* **2022**, *9*, No. 866719.
(12) Rodrigues, T.; Reker, D.; Schneider, P.; Schneider, G. Counting on Natural Products for Drug Design. *Nat. Chem.* **2016**, *8* (6), 531−541.
(13) Xiong, H.-H.; Lin, S.-Y.; Chen, L.-L.; Ouyang, K.-H.; Wang, W.-J. The Interaction between Flavonoids and Intestinal Microbes: A Review. *Foods* **2023**, *12* (2), 320.
(14) Jaikaran, E. T. A. S.; Clark, A. Islet Amyloid and Type 2 Diabetes: From Molecular Misfolding to Islet Pathophysiology. *Biochim. Biophys. Acta, Mol. Basis Dis.* **2001**, *1537* (3), 179−203.
(15) Nedumpully-Govindan, P.; Kakinen, A.; Pilkington, E. H.; Davis, T. P.; Chun Ke, P.; Ding, F. Stabilizing Off-Pathway Oligomers by Polyphenol Nanoassemblies for IAPP Aggregation Inhibition. *Sci. Rep.* **2016**, *6* (1), No. 19463.
(16) Bondonno, N. P.; Dalgaard, F.; Murray, K.; Davey, R. J.; Bondonno, C. P.; Cassidy, A.; Lewis, J. R.; Kyrø, C.; Gislason, G.; Scalbert, A.; Tjønneland, A.; Hodgson, J. M. Higher Habitual Flavonoid Intakes Are Associated with a Lower Incidence of Diabetes. *J. Nutr.* **2021**, *151* (11), 3533−3542.
(17) Schaduangrat, N.; Lampa, S.; Simeon, S.; Gleeson, M. P.; Spjuth, O.; Nantasenamat, C. Towards Reproducible Computational Drug Discovery. *J. Cheminf.* **2020**, *12* (1), No. 9.
(18) Vora, D. S.; Kalakoti, Y.; Sundar, D. Computational Methods and Deep Learning for Elucidating Protein Interaction Networks. In *Computational Biology and Machine Learning for Metabolic Engineering and Synthetic Biology*; Selvarajoo, K., Ed.; Methods in Molecular Biology; Springer US: New York, NY, 2023; Vol. *2553*, pp 285−323.
(19) Sliwoski, G.; Kothiwale, S.; Meiler, J.; Lowe, E. W. Computational Methods in Drug Discovery. *Pharmacol. Rev.* **2014**, *66* (1), 334−395.
(20) Messaoudi, A.; Belguith, H.; Ben Hamida, J. Homology Modeling and Virtual Screening Approaches to Identify Potent Inhibitors of VEB-1 β-Lactamase. *Theor. Biol. Med. Model.* **2013**, *10* (1), No. 22.
(21) Colovos, C.; Yeates, T. O. Verification of Protein Structures: Patterns of Nonbonded Atomic Interactions. *Protein Sci.* **1993**, *2* (9), 1511−1519.
(22) Basnet, S.; Ghimire, M. P.; Lamichhane, T. R.; Adhikari, R.; Adhikari, A. Identification of Potential Human Pancreatic α-Amylase Inhibitors from Natural Products by Molecular Docking, MM/GBSA Calculations, MD Simulations, and ADMET Analysis. *PLoS One* **2023**, *18* (3), No. e0275765.
(23) Mohan, M.; Anindya, R. Elucidation of the Molecular Interactions That Enable Stable Interaction between HIV Protease Inhibitor Ritonavir and Human DNA Repair Enzyme ALKBH2: A Molecular Dynamics Simulation Study. *bioRxiv* **2021**, DOI: 10.1101/2021.09.26.461894.
(24) Halgren, T. A. Identifying and Characterizing Binding Sites and Assessing Druggability. *J. Chem. Inf. Model.* **2009**, *49* (2), 377−389.
(25) Chauhan, N.; Gajjar, A. Classifying Druggability on Potential Binding Sites of Glycogen Synthase Kinase-3?: An in-Silico Assessment. *Acta Pharm. Sci.* **2017**, *55* (3), 43.
(26) Meng, Y.; Su, A.; Yuan, S.; Zhao, H.; Tan, S.; Hu, C.; Deng, H.; Guo, Y. Evaluation of Total Flavonoids, Myricetin, and Quercetin from Hovenia Dulcis Thunb. As Inhibitors of α-Amylase and α-Glucosidase. *Plant Foods Hum. Nutr.* **2016**, *71* (4), 444−449.
(27) De Vivo, M.; Masetti, M.; Bottegoni, G.; Cavalli, A. Role of Molecular Dynamics and Related Methods in Drug Discovery. *J. Med. Chem.* **2016**, *59* (9), 4035−4061.
(28) Silveira, A. C.; Dias, J. P.; Santos, V. M.; Oliveira, P. F.; Alves, M. G.; Rato, L.; Silva, B. M. The Action of Polyphenols in Diabetes Mellitus and Alzheimer's Disease: A Common Agent for Overlapping Pathologies. *CN* **2019**, *17* (7), 590−613.
(29) Zhao, C.; Wan, X.; Zhou, S.; Cao, H. Natural Polyphenols: A Potential Therapeutic Approach to Hypoglycemia. *eFood* **2020**, *1* (2), 107−118.
(30) Guasch-Ferré, M.; Merino, J.; Sun, Q.; Fitó, M.; Salas-Salvadó, J. Dietary Polyphenols, Mediterranean Diet, Prediabetes, and Type 2 Diabetes: A Narrative Review of the Evidence. *Oxid. Med. Cell. Longevity* **2017**, *2017*, 1−16.
(31) Nie, T.; Cooper, G. J. S. Mechanisms Underlying the Antidiabetic Activities of Polyphenolic Compounds: A Review. *Front. Pharmacol.* **2021**, *12*, No. 798329.
(32) Matacchione, G.; Gurău, F.; Baldoni, S.; Prattichizzo, F.; Silvestrini, A.; Giuliani, A.; Pugnaloni, A.; Espinosa, E.; Amenta, F.; Bonafè, M.; Procopio, A. D.; Rippo, M. R.; Olivieri, F.; Sabbatinelli, J. Pleiotropic Effects of Polyphenols on Glucose and Lipid Metabolism: Focus on Clinical Trials. *Ageing Res. Rev.* **2020**, *61*, No. 101074.
(33) Kumar Singh, A.; Cabral, C.; Kumar, R.; Ganguly, R.; Kumar Rana, H.; Gupta, A.; Rosaria Lauro, M.; Carbone, C.; Reis, F.; Pandey, A. K. Beneficial Effects of Dietary Polyphenols on Gut Microbiota and Strategies to Improve Delivery Efficiency. *Nutrients* **2019**, *11* (9), 2216.
(34) Umar, H. I.; Josiah, S. S.; Saliu, T. P.; Jimoh, T. O.; Ajayi, A.; Danjuma, J. B. In-Silico Analysis of the Inhibition of the SARS-CoV-2 Main Protease by Some Active Compounds from Selected African Plants. *J. Taibah Univ. Med. Sci.* **2021**, *16* (2), 162−176.
(35) Laaraj, N.; Bouhrim, M.; Kharchoufa, L.; Tiji, S.; Bendaha, H.; Addi, M.; Drouet, S.; Hano, C.; Lorenzo, J. M.; Bnouham, M.; Mimouni, M. Phytochemical Analysis, α-Glucosidase and α-Amylase Inhibitory Activities and Acute Toxicity Studies of Extracts from Pomegranate (Punica Granatum) Bark, a Valuable Agro-Industrial By-Product. *Foods* **2022**, *11* (9), 1353.
(36) Kikiowo, B.; Ahmad, I.; Alade, A. A.; T Ijatuyi, T.; Iwaloye, O.; Patel, H. M. Molecular Dynamics Simulation and Pharmacokinetics Studies of Ombuin and Quercetin against Human Pancreatic α-Amylase. *J. Biomol. Struct. Dyn.* **2022**, 1−8.
(37) Kulkarni, S.; Dwivedi, P.; Danappanvar, A. N.; Subhash, B. A.; Patil, B. M. Identification of α-Amylase Inhibitors from Flavonoid Fraction of Feronia Elephantum and Its Integration with in-Silico Studies. *In Silico Pharmacol.* **2021**, *9* (1), No. 50.
(38) Durrant, J. D.; McCammon, J. A. Molecular Dynamics Simulations and Drug Discovery. *BMC Biol.* **2011**, *9* (1), No. 71.
(39) Mollica, L.; Theret, I.; Antoine, M.; Perron-Sierra, F.; Charton, Y.; Fourquez, J.-M.; Wierzbicki, M.; Boutin, J. A.; Ferry, G.; Decherchi, S.; Bottegoni, G.; Ducrot, P.; Cavalli, A. Molecular Dynamics Simulations and Kinetic Measurements to Estimate and Predict Protein−Ligand Residence Times. *J. Med. Chem.* **2016**, *59* (15), 7167−7176.
(40) Ahmed, S.; Ali, M.; Ruma, R.; Mahmud, S.; Paul, G.; Saleh, M.; Alshahrani, M.; Obaidullah, A.; Biswas, S.; Rahman, M.; Rahman, M.; Islam, M. Molecular Docking and Dynamics Simulation of Natural Compounds from Betel Leaves (Piper Betle L.) for Investigating the Potential Inhibition of Alpha-Amylase and Alpha-Glucosidase of Type 2 Diabetes. *Molecules* **2022**, *27* (14), 4526.
(41) Sharma, P.; Joshi, T.; Joshi, T.; Chandra, S.; Tamta, S. Molecular Dynamics Simulation for Screening Phytochemicals as α-Amylase Inhibitors from Medicinal Plants. *J. Biomol. Struct. Dyn.* **2021**, *39* (17), 6524−6538.
(42) Abchir, O.; Daoui, O.; Belaidi, S.; Ouassaf, M.; Qais, F. A.; ElKhattabi, S.; Belaaouad, S.; Chtita, S. Design of Novel Benzimidazole Derivatives as Potential α-Amylase Inhibitors Using QSAR, Pharmacokinetics, Molecular Docking, and Molecular Dynamics Simulation Studies. *J. Mol. Model.* **2022**, *28* (4), No. 106.
(43) Abu Bakar, A. R.; Manaharan, T.; Merican, A. F.; Mohamad, S. B. Experimental and Computational Approaches to Reveal the Potential of *Ficus Deltoidea* Leaves Extract as α-Amylase Inhibitor. *Nat. Prod. Res.* **2018**, *32* (4), 473−476.

https://doi.org/10.1021/acsomega.3c05082
ACS Omega 2023, 8, 43617−43631

(44) Kamaraj, B.; Rajendran, V.; Sethumadhavan, R.; Kumar, C. V.; Purohit, R. Mutational Analysis of FUS Gene and Its Structural and Functional Role in Amyotrophic Lateral Sclerosis 6. *J. Biomol. Struct. Dyn.* **2015**, *33* (4), 834−844.
(45) Hou, T.; Wang, J.; Li, Y.; Wang, W. Assessing the Performance of the Molecular Mechanics/Poisson Boltzmann Surface Area and Molecular Mechanics/Generalized Born Surface Area Methods. II. The Accuracy of Ranking Poses Generated from Docking. *J. Comput. Chem.* **2011**, *32* (5), 866−877.
(46) Pattar, S. V.; Adhoni, S. A.; Kamanavalli, C. M.; Kumbar, S. S. In Silico Molecular Docking Studies and MM/GBSA Analysis of Coumarin-Carbonodithioate Hybrid Derivatives Divulge the Anti-cancer Potential against Breast Cancer. *Beni-Suef Univ. J. Basic Appl. Sci.* **2020**, *9* (1), No. 36.
(47) Martinez-Gonzalez, A. I.; Díaz-Sánchez, Á. G.; De La Rosa, L. A.; Bustos-Jaimes, I.; Alvarez-Parrilla, E. Inhibition of α-Amylase by Flavonoids: Structure Activity Relationship (SAR). *Spectrochim. Acta, Part A* **2019**, *206*, 437−447.
(48) Shen, H.; Wang, J.; Ao, J.; Hou, Y.; Xi, M.; Cai, Y.; Li, M.; Luo, A. Structure-Activity Relationships and the Underlying Mechanism of α-Amylase Inhibition by Hyperoside and Quercetin: Multi-Spectroscopy and Molecular Docking Analyses. *Spectrochim. Acta, Part A* **2023**, *285*, No. 121797.
(49) S M Abd El-Kareem, M.; A Rabbih, M.; Elansary, H. O.; A Al-Mana, F. Mass Spectral Fragmentation of Pelargonium Graveolens Essential Oil Using GC−MS Semi-Empirical Calculations and Biological Potential. *Processes* **2020**, *8* (2), 128.
(50) Huang, Y.; Rong, C.; Zhang, R.; Liu, S. Evaluating Frontier Orbital Energy and HOMO/LUMO Gap with Descriptors from Density Functional Reactivity Theory. *J. Mol. Model.* **2017**, *23* (1), No. 3.
(51) Kumar, C. B. P.; Raghu, M. S.; Prasad, K. N. N.; Chandrasekhar, S.; Jayanna, B. K.; Alharthi, F. A.; Prashanth, M. K.; Kumar, K. Y. Investigation of Biological Activity of 2,3-Disubstituted Quinazolin-4(1 *H*)-Ones against *Mycobacterium Tuberculosis* and DNA *via* Docking, Spectroscopy and DFT Studies. *New J. Chem.* **2021**, *45* (1), 403−414.
(52) De Proft, F.; Geerlings, P. Conceptual and Computational DFT in the Study of Aromaticity. *Chem. Rev.* **2001**, *101* (5), 1451−1464.
(53) Veiko, A. G.; Lapshina, E. A.; Zavodnik, I. B. Comparative Analysis of Molecular Properties and Reactions with Oxidants for Quercetin, Catechin, and Naringenin. *Mol. Cell. Biochem.* **2021**, *476* (12), 4287−4299.
(54) Singh, J. S.; Khan, M. S.; Uddin, S. A DFT Study of Vibrational Spectra of 5-Chlorouracil with Molecular Structure, HOMO−LUMO, MEPs/ESPs and Thermodynamic Properties. *Polym. Bull.* **2023**, *80* (3), 3055−3083.
(55) Erdogan, T. *In-Silico* Investigation of Some Recent Natural Compounds for Their Potential Use against SARS-CoV-2: A DFT, Molecular Docking and Molecular Dynamics Study. *J. Biomol. Struct. Dyn.* **2023**, *41* (6), 2448−2465.
(56) Hefti, F. F. Requirements for a Lead Compound to Become a Clinical Candidate. *BMC Neurosci.* **2008**, *9* (S3), No. S7.
(57) Paul, S. M.; Mytelka, D. S.; Dunwiddie, C. T.; Persinger, C. C.; Munos, B. H.; Lindborg, S. R.; Schacht, A. L. How to Improve R&D Productivity: The Pharmaceutical Industry's Grand Challenge. *Nat. Rev. Drug Discovery* **2010**, *9* (3), 203−214.
(58) Lagorce, D.; Douguet, D.; Miteva, M. A.; Villoutreix, B. O. Computational Analysis of Calculated Physicochemical and ADMET Properties of Protein-Protein Interaction Inhibitors. *Sci. Rep.* **2017**, *7* (1), No. 46277.
(59) Muehlbacher, M.; Spitzer, G. M.; Liedl, K. R.; Kornhuber, J. Qualitative Prediction of Blood−Brain Barrier Permeability on a Large and Refined Dataset. *J. Comput. Aided Mol. Des.* **2011**, *25* (12), 1095−1106.
(60) Faria, A.; Pestana, D.; Teixeira, D.; Azevedo, J.; Freitas, V.; Mateus, N.; Calhau, C. Flavonoid Transport across RBE4 Cells: A Blood-Brain Barrier Model. *Cell. Mol. Biol. Lett.* **2010**, *15* (2), 234−241, DOI: 10.2478/s11658-010-0006-4.
(61) Schaffer, S.; Halliwell, B. Do Polyphenols Enter the Brain and Does It Matter? Some Theoretical and Practical Considerations. *Genes Nutr.* **2012**, *7* (2), 99−109.
(62) Bibi, Z. Role of Cytochrome P450 in Drug Interactions. *Nutr. Metab.* **2008**, *5* (1), No. 27.
(63) Giacomini, K. M.; Huang, S.-M.; Tweedie, D. J.; Benet, L. Z.; Brouwer, K. L. R.; Chu, X.; Dahlin, A.; Evers, R.; Fischer, V.; Hillgren, K. M.; Hoffmaster, K. A.; Ishikawa, T.; Keppler, D.; Kim, R. B.; Lee, C. A.; Niemi, M.; Polli, J. W.; Sugiyama, Y.; Swaan, P. W.; Ware, J. A.; Wright, S. H.; Wah Yee, S.; Zamek-Gliszczynski, M. J.; Zhang, L.; The International Transporter Consortium. Membrane Transporters in Drug Development. *Nat. Rev. Drug Discovery* **2010**, 215−236, DOI: 10.1038/nrd3028.
(64) Wu, L.-X.; Guo, C.-X.; Chen, W.-Q.; Yu, J.; Qu, Q.; Chen, Y.; Tan, Z.-R.; Wang, G.; Fan, L.; Li, Q.; Zhang, W.; Zhou, H.-H. Inhibition of the Organic Anion-Transporting Polypeptide 1B1 by Quercetin: An in Vitro and in Vivo Assessment: Effect of Quercetin on the Pharmacokinetics of the OATP1B1 Substrate, Pravastatin. *Br. J. Clin. Pharmacol.* **2012**, *73* (5), 750−757.
(65) Xu, C.; Cheng, F.; Chen, L.; Du, Z.; Li, W.; Liu, G.; Lee, P. W.; Tang, Y. In Silico Prediction of Chemical Ames Mutagenicity. *J. Chem. Inf. Model.* **2012**, *52* (11), 2840−2847.
(66) Al-Nour, M. Y.; Ibrahim, M. M.; Elsaman, T. Ellagic Acid, Kaempferol, and Quercetin from Acacia Nilotica: Promising Combined Drug With Multiple Mechanisms of Action. *Curr. Pharmacol. Rep.* **2019**, *5* (4), 255−280.
(67) Mendoza-Wilson, A. M.; Glossman-Mitnik, D. CHIH-DFT Study of the Electronic Properties and Chemical Reactivity of Quercetin. *J. Mol. Struct.: THEOCHEM* **2005**, *716* (1−3), 67−72.
(68) Singh, S. P.; Konwar, B. K. Molecular Docking Studies of Quercetin and Its Analogues against Human Inducible Nitric Oxide Synthase. *SpringerPlus* **2012**, *1* (1), No. 69.
(69) Hasan, M. M.; Khan, Z.; Chowdhury, M. S.; Khan, M. A.; Moni, M. A.; Rahman, M. H. In Silico Molecular Docking and ADME/T Analysis of Quercetin Compound with Its Evaluation of Broad-Spectrum Therapeutic Potential against Particular Diseases. *Inf. Med. Unlocked* **2022**, *29*, No. 100894.
(70) Ghose, A. K.; Viswanadhan, V. N.; Wendoloski, J. J. A Knowledge-Based Approach in Designing Combinatorial or Medicinal Chemistry Libraries for Drug Discovery. 1. A Qualitative and Quantitative Characterization of Known Drug Databases. *J. Comb. Chem.* **1999**, *1* (1), 55−68.
(71) Lipinski, C. A. Drug-like Properties and the Causes of Poor Solubility and Poor Permeability. *J. Pharmacol. Toxicol. Methods* **2000**, *44* (1), 235−249.
(72) Doak, B. C.; Over, B.; Giordanetto, F.; Kihlberg, J. Oral Druggable Space beyond the Rule of 5: Insights from Drugs and Clinical Candidates. *Chem. Biol.* **2014**, *21* (9), 1115−1142.
(73) Egan, W. J.; Merz, K. M.; Baldwin, J. J. Prediction of Drug Absorption Using Multivariate Statistics. *J. Med. Chem.* **2000**, *43* (21), 3867−3877.
(74) Mohamed, G. A.; Omar, A. M.; El-Araby, M. E.; Mass, S.; Ibrahim, S. R. M. Assessments of Alpha-Amylase Inhibitory Potential of Tagetes Flavonoids through In Vitro, Molecular Docking, and Molecular Dynamics Simulation Studies. *IJMS* **2023**, *24* (12), 10195.
(75) Oboh, G.; Ademosun, A. O.; Ayeni, P. O.; Omojokun, O. S.; Bello, F. Comparative Effect of Quercetin and Rutin on α-Amylase, α-Glucosidase, and Some pro-Oxidant-Induced Lipid Peroxidation in Rat Pancreas. *Comp. Clin. Pathol.* **2015**, *24* (5), 1103−1110.
(76) Darnis, S.; Juge, N.; Guo, X.-J.; Marchis-Mouren, G.; Puigserver, A.; Chaix, J.-C. Molecular Cloning and Primary Structure Analysis of Porcine Pancreatic α-Amylase. *Biochim. Biophys. Acta, Protein Struct. Mol. Enzymol.* **1999**, *1430* (2), 281−289.
(77) Sun, L.; Wang, Y.; Miao, M. Inhibition of α-Amylase by Polyphenolic Compounds: Substrate Digestion, Binding Interactions and Nutritional Intervention. *Trends Food Sci. Technol.* **2020**, *104*, 190−207.
(78) Ansari, P.; Choudhury, S. T.; Seidel, V.; Rahman, A. B.; Aziz, Md. A.; Richi, A. E.; Rahman, A.; Jafrin, U. H.; Hannan, J. M. A.;

https://doi.org/10.1021/acsomega.3c05082
ACS Omega 2023, 8, 43617−43631

Abdel-Wahab, Y. H. A. Therapeutic Potential of Quercetin in the Management of Type-2 Diabetes Mellitus. *Life* **2022**, *12* (8), 1146.
(79) Sultana, B.; Anwar, F. Flavonols (Kaempeferol, Quercetin, Myricetin) Contents of Selected Fruits, Vegetables and Medicinal Plants. *Food Chem.* **2008**, *108* (3), 879−884.
(80) Vásquez-Garzón, V. R.; Arellanes-Robledo, J.; García-Román, R.; Aparicio-Rautista, D. I.; Villa-Treviño, S. Inhibition of Reactive Oxygen Species and Pre-Neoplastic Lesions by Quercetin through an Antioxidant Defense Mechanism. *Free Radical Res.* **2009**, *43* (2), 128−137.
(81) Ramos, F. A.; Takaishi, Y.; Shirotori, M.; Kawaguchi, Y.; Tsuchiya, K.; Shibata, H.; Higuti, T.; Tadokoro, T.; Takeuchi, M. Antibacterial and Antioxidant Activities of Quercetin Oxidation Products from Yellow Onion (*Allium Cepa*) Skin. *J. Agric. Food Chem.* **2006**, *54* (10), 3551−3557.
(82) Anand David, A.; Arulmoli, R.; Parasuraman, S. Overviews of Biological Importance of Quercetin: A Bioactive Flavonoid. *Phcog. Rev.* **2016**, *10* (20), 84.
(83) Darenskaya, M. A.; Kolesnikova, L. I.; Kolesnikov, S. I. Oxidative Stress: Pathogenetic Role in Diabetes Mellitus and Its Complications and Therapeutic Approaches to Correction. *Bull. Exp. Biol. Med.* **2021**, *171* (2), 179−189.
(84) Kaneto, H.; Katakami, N.; Matsuhisa, M.; Matsuoka, T. Role of Reactive Oxygen Species in the Progression of Type 2 Diabetes and Atherosclerosis. *Mediators Inflammation* **2010**, *2010*, 1−11.
(85) Salehi, B.; Machin, L.; Monzote, L.; Sharifi-Rad, J.; Ezzat, S. M.; Salem, M. A.; Merghany, R. M.; El Mahdy, N. M.; Kılıç, C. S.; Sytar, O.; Sharifi-Rad, M.; Sharopov, F.; Martins, N.; Martorell, M.; Cho, W. C. Therapeutic Potential of Quercetin: New Insights and Perspectives for Human Health. *ACS Omega* **2020**, *5* (20), 11849−11872.
(86) Singh, J.; Mittal, P.; Vasant Bonde, G.; Ajmal, G.; Mishra, B. Design, Optimization, Characterization and in-Vivo Evaluation of Quercetin Enveloped Soluplus/P407 Micelles in Diabetes Treatment. *Artif. Cells, Nanomed., Biotechnol.* **2018**, *46* (sup3), S546−S555.
(87) Gadakar, P. K.; Phukan, S.; Dattatreya, P.; Balaji, V. N. Pose Prediction Accuracy in Docking Studies and Enrichment of Actives in the Active Site of GSK-3β. *J. Chem. Inf. Model.* **2007**, *47* (4), 1446−1459.
(88) Lu, C.; Wu, C.; Ghoreishi, D.; Chen, W.; Wang, L.; Damm, W.; Ross, G. A.; Dahlgren, M. K.; Russell, E.; Von Bargen, C. D.; Abel, R.; Friesner, R. A.; Harder, E. D. OPLS4: Improving Force Field Accuracy on Challenging Regimes of Chemical Space. *J. Chem. Theory Comput.* **2021**, *17* (7), 4291−4300.
(89) Madhavi Sastry, G.; Adzhigirey, M.; Day, T.; Annabhimoju, R.; Sherman, W. Protein and Ligand Preparation: Parameters, Protocols, and Influence on Virtual Screening Enrichments. *J. Comput.-Aided Mol. Des.* **2013**, *27* (3), 221−234.
(90) Jacobson, M. P.; Pincus, D. L.; Rapp, C. S.; Day, T. J. F.; Honig, B.; Shaw, D. E.; Friesner, R. A. A Hierarchical Approach to All-Atom Protein Loop Prediction. *Proteins* **2004**, *55* (2), 351−367.
(91) Rapp, C.; Kalyanaraman, C.; Schiffmiller, A.; Schoenbrun, E. L.; Jacobson, M. P. A Molecular Mechanics Approach to Modeling Protein−Ligand Interactions: Relative Binding Affinities in Congeneric Series. *J. Chem. Inf. Model.* **2011**, *51* (9), 2082−2089.
(92) Friesner, R. A.; Murphy, R. B.; Repasky, M. P.; Frye, L. L.; Greenwood, J. R.; Halgren, T. A.; Sanschagrin, P. C.; Mainz, D. T. Extra Precision Glide: Docking and Scoring Incorporating a Model of Hydrophobic Enclosure for Protein−Ligand Complexes. *J. Med. Chem.* **2006**, *49* (21), 6177−6196.
(93) Elekofehinti, O. O.; Ejelonu, O. C.; Kamdem, J. P.; Akinlosotu, O. B.; Famuti, A.; Adebowale, D. D.; Iwaloye, O.; Bulu, Y. I.; Kade, I. J.; Rocha, J. B. T. Discovery of Potential Visfatin Activators Using in Silico Docking and ADME Predictions as Therapy for Type 2 Diabetes. *Beni-Suef Univ. J. Basic App. Sci.* **2018**, *7* (2), 241−249.
(94) Li, J.; Abel, R.; Zhu, K.; Cao, Y.; Zhao, S.; Friesner, R. A. The VSGB 2.0 Model: A next Generation Energy Model for High Resolution Protein Structure Modeling: The VSGB 2.0 Energy Model. *Proteins* **2011**, *79* (10), 2794−2812.
(95) Ganesan, A.; Coote, M. L.; Barakat, K. Molecular Dynamics-Driven Drug Discovery: Leaping Forward with Confidence. *Drug Discovery Today* **2017**, *22* (2), 249−269.
(96) Abraham, M. J.; Murtola, T.; Schulz, R.; Páll, S.; Smith, J. C.; Hess, B.; Lindahl, E. GROMACS: High Performance Molecular Simulations through Multi-Level Parallelism from Laptops to Supercomputers. *SoftwareX* **2015**, *1−2*, 19−25.
(97) Khan, F. I.; Song, H.; Hassan, F.; Tian, J.; Tang, L.; Lai, D.; Juan, F. Impact of Amino Acid Substitutions on the Behavior of a Photoactivatable near Infrared Fluorescent Protein PAiRFP1. *Spectrochim. Acta, Part A* **2021**, *253*, No. 119572.
(98) Mark, P.; Nilsson, L. Structure and Dynamics of the TIP3P, SPC, and SPC/E Water Models at 298 K. *J. Phys. Chem. A* **2001**, *105* (43), 9954−9960.
(99) Schüttelkopf, A. W.; Van Aalten, D. M. F. *PRODRG* : A Tool for High-Throughput Crystallography of Protein−Ligand Complexes. *Acta Crystallogr., Sect. D: Biol. Crystallogr.* **2004**, *60* (8), 1355−1363.
(100) Izadi, S.; Anandakrishnan, R.; Onufriev, A. V. Building Water Models: A Different Approach. *J. Phys. Chem. Lett.* **2014**, *5* (21), 3863−3871.
(101) Ross, G. A.; Rustenburg, A. S.; Grinaway, P. B.; Fass, J.; Chodera, J. D. Biomolecular Simulations under Realistic Macroscopic Salt Conditions. *J. Phys. Chem. B* **2018**, *122* (21), 5466−5486.
(102) Tuble, S. C.; Anwar, J.; Gale, J. D. An Approach to Developing a Force Field for Molecular Simulation of Martensitic Phase Transitions between Phases with Subtle Differences in Energy and Structure. *J. Am. Chem. Soc.* **2004**, *126* (1), 396−405.
(103) Gill, P. M. W.; Johnson, B. G.; Pople, J. A.; Frisch, M. J. The Performance of the Becke—Lee—Yang—Parr (B—LYP) Density Functional Theory with Various Basis Sets. *Chem. Phys. Lett.* **1992**, *197* (4−5), 499−505.
(104) Pandey, A. K.; Bajpai, A.; Baboo, V.; Dwivedi, A. Structural, Electronic, and Vibrational Properties of Isoniazid and Its Derivative N-Cyclopentylidenepyridine-4-Carbohydrazide: A Quantum Chemical Study. *J. Theor. Chem.* **2014**, *2014*, 1−15.
(105) Dwivedi, A.; Baboo, V.; Bajpai, A. Fukui Function Analysis and Optical, Electronic, and Vibrational Properties of Tetrahydrofuran and Its Derivatives: A Complete Quantum Chemical Study. *J. Theor. Chem.* **2015**, *2015*, 1−11.
(106) Yang, H.; Lou, C.; Sun, L.; Li, J.; Cai, Y.; Wang, Z.; Li, W.; Liu, G.; Tang, Y. AdmetSAR 2.0: Web-Service for Prediction and Optimization of Chemical ADMET Properties. *Bioinformatics* **2019**, *35* (6), 1067−1069.
(107) Pires, D. E. V.; Blundell, T. L.; Ascher, D. B. PkCSM: Predicting Small-Molecule Pharmacokinetic and Toxicity Properties Using Graph-Based Signatures. *J. Med. Chem.* **2015**, *58* (9), 4066−4072.
(108) Daina, A.; Michielin, O.; Zoete, V. SwissADME: A Free Web Tool to Evaluate Pharmacokinetics, Drug-Likeness and Medicinal Chemistry Friendliness of Small Molecules. *Sci. Rep.* **2017**, *7* (1), No. 42717.
(109) Senger, M. R.; Gomes, L. D. C. A.; Ferreira, S. B.; Kaiser, C. R.; Ferreira, V. F.; Silva, F. P. Kinetics Studies on the Inhibition Mechanism of Pancreatic α-Amylase by Glycoconjugated 1H-1,2,3-Triazoles: A New Class of Inhibitors with Hypoglycemiant Activity. *ChemBioChem* **2012**, *13* (11), 1584−1593.

https://doi.org/10.1021/acsomega.3c05082
ACS Omega 2023, 8, 43617−43631